CD8+ T cell–Dependent Remodeling of the Tumor Microenvironment Overcomes Chemoresistance

Liyan Lao[1,2,3], Wenfeng Zeng[1,2,3], Penghan Huang[1,2,3], Huiping Chen[1,2,3], Zishuo Jia[1,2,3], Pei Wang[1,2,3], Di Huang[1,2,3], Jianing Chen[1,2,3], Yan Nie[1,2,3], Linbin Yang[1,2,3], Wei Wu[1,2,3], and Jiang Liu[1,2,3]

ABSTRACT

The therapeutic efficacy of chemotherapy is in part a result of its ability to enhance adaptive antitumor immune responses. However, tumor cells exploit various evasion mechanisms to escape the immune attack and blunt chemosensitivity. Herein, we report that through single-cell profiling of the tumor immune microenvironment, we identified a subset of CD161-overexpressing CD8+ T cells enriched in chemoresistant tumors. CD161 engagement repressed the calcium influx and cytolytic capacity of CD8+ T cells through acid sphingomyelinase activation and ceramide generation. Targeting CD161 in adoptively transferred cytotoxic T lymphocytes enhanced antitumor immunity and reversed chemoresistance in patient-derived xenografts in vivo. Clinically, CD161 expression on CD8+ T cells was associated with chemoresistance and shortened patient survival. Our findings provide insights into novel immunosuppressive mechanisms in chemoresistance and highlight targeting CD161 as a potential therapeutic strategy.

Introduction

Despite achieving clinical benefits in some patients, conventional antitumor chemotherapy regimens face nonnegligible challenges, among which chemoresistance continues to be the principal limiting factor for achieving cures in patients with cancer (1–3). Increasing evidence has shown that in addition to directly affecting neoplastic cells, chemotherapy can enhance adaptive antitumor immunity either by inducing immunogenic cell death and activating effector T cells or by inhibiting immunosuppressive cells and augmenting T-cell infiltration into tumors (4–7). However, tumor cells can evade the immune-related benefits of chemotherapy and continue to progress by remodeling the intricate tumor microenvironment to their own advantage and subverting antitumor immune surveillance (8, 9). Therefore, in recent years, new strategies of combining chemotherapy with immunotherapy, such as immune-checkpoint blockade, have been proposed and shown promise in improving chemosensitivity in clinical practice (10–12). Unfortunately, substantial individual variability is seen in treatment efficacy, and many patients do not benefit from the combination therapies (10–12), suggesting that in addition to the well-known immune checkpoints, there are still some enigmatic immune evasion mechanisms involved in nonresponsiveness to chemotherapy. As a consequence, there is an urgent need for a comprehensive dissection of the chemoresistant tumor immune microenvironment and a detailed analysis of all cell subsets and molecules with a possible role in immune escape to achieve precise targeting of chemoresistance mechanisms and complete reversal of nonresponsiveness to chemotherapy.

Here, we report single-cell dissection of tumor-infiltrating immune cell heterogeneity in chemosensitive and chemoresistant breast cancer patients. We identified a distinct CD8+ T-cell subset enriched in chemoresistant tumors and showed how this population affects antitumor immunity and responses to chemotherapy.

Materials and Methods

Patients and samples

Samples were collected from 535 patients undergoing breast surgeries at the Sun Yat-Sen Memorial Hospital, Sun Yat-Sen University between 2008 and 2020. After a definite diagnosis with puncture specimens, all the patients received neoadjuvant chemotherapy. Tumor samples obtained via large core-needle biopsy before neoadjuvant chemotherapy were kept in paraffin blocks for all patients. For patients in the discovery cohort (10 cases), validation cohort 1 (18 cases), and some patients in validation cohort 2 (48 cases), part of the biopsy specimens were dissociated for single-cell suspensions and preserved in liquid nitrogen for subsequent RNA sequencing (RNA-seq), flow cytometry, polymerase chain reaction (PCR), or western blot analyses (Supplementary Fig. S1A). After 6 to 8 courses of neoadjuvant chemotherapy, breast cancer patients underwent surgical tumor resection. For all patients, surgically removed tumor samples were collected and stored in paraffin blocks. The neoadjuvant chemotherapeutic regimens were as follows: four cycles of doxorubicin 60 mg/m^2 plus cyclophosphamide 600 mg/m^2 (AC) every 3 weeks, followed by paclitaxel (80 mg/m^2) weekly for 12 weeks; or four cycles of docetaxel 75 mg/m^2 plus cyclophosphamide 600 mg/m^2 (TC) every 3 weeks. The therapeutic efficacy of neoadjuvant chemotherapy was evaluated based on Response Evaluation Criteria in Solid Tumors (RECIST). Complete remission (CR) and partial remission (PR) were classified as chemotherapy-sensitive, whereas stable disease (SD) and progressive disease (PD) were classified as chemotherapy-resistant. All experiments using human samples in this research were performed in

[1]Guangdong Provincial Key Laboratory of Malignant Tumor Epigenetics and Gene Regulation, Medical Research Center, Sun Yat-Sen Memorial Hospital, Sun Yat-Sen University, Guangzhou, China. [2]Breast Tumor Center, Sun Yat-Sen Memorial Hospital, Sun Yat-Sen University, Guangzhou, China. [3]Bioland Laboratory, Guangzhou, China.

L. Lao and W. Zeng contributed equally to this article.

Corresponding Author: Jiang Liu, Department of Breast Tumor Center, Sun-Yat-Sen Memorial Hospital, Sun-Yat-Sen University, 107 Yanjiang West Road, Guangzhou, 510120, P.R. China. Phone: 8620-8733-2022; Fax: 8620-8133-2576; E-mail: liuj658@mail.sysu.edu.cn; Wei Wu, 8620-8733-2022; E-mail: wuwei7@mail.sysu.edu.cn; Linbin Yang, 8620-8733-2022; E-mail: yanglinb123@163.com; and Yan Nie, 8620-8733-2022; E-mail: nieyan1010@163.com

accordance with the Declaration of Helsinki. All data related to clinical samples were approved by the internal review and ethics board of Sun Yat-Sen Memorial Hospital, and informed written consent for the use of samples for research purposes was obtained from patients.

Primary cell isolation from tumor tissue

Primary CD45$^+$ immune cells, CD8$^+$ tumor-infiltrating lymphocytes (TIL), and breast cancer cells were isolated from breast carcinoma samples obtained from biopsies or surgery. Briefly, tissues were cut into fragments of approximately 1 mm^3 and then digested by enzymatic hydrolysate [DMEM (Gibco, #C11995500BT) supplemented with 10% FBS (Gibco, #10099141C), 1.5 mg/mL collagenase type I (Worthington, #LS004196), 1.5 mg/mL collagenase type III (Worthington, #LS004182), and 1.5 mg/mL hyaluronidase (Sigma-Aldrich, #H3506)] at 37°C with gentle agitation for 2 hours for cancer cell isolation and 1 hour for immune cell isolation. The dissociated tissues were resuspended and filtered through a 70-μm cell strainer to obtain single-cell suspensions. Thereafter, cancer cells were acquired through centrifugation at 250 × g for 5 minutes and purified using EpCAM Microbeads (Miltenyi Biotec, #130-061-101). To isolate immune cells, primary cell suspensions were centrifuged at 400 × g for 5 minutes and then CD8$^+$ TILs were purified using CD8 Microbeads (Miltenyi Biotec, #130-045-201). CD45$^+$ immune cells were isolated by fluorescence-activated cell sorting (FACS) using a BD Influx flow cytometer (see "FACS"). After isolation, cell purity was determined by flow cytometry (>95%).

Cell culture

Isolated primary cancer cells were cultured in DMEM (Gibco, #C11995500BT) supplemented with 10% FBS (Gibco, # 10099141C) and immune cells in RPMI-1640 (Gibco, #C11875500BT) supplemented with 10% FBS and 25 U/mL IL2 (PeproTech, #200-02). Cell lines MDA-MB-231, SaoS2, and MCF-7 were obtained from the American Type Culture Collection (https://www.atcc.org) in 2019 to 2022 and cultured in DMEM supplemented with 10% FBS. Experiments were performed with cells passaged between 5 and 20 times. All the cell lines were reauthenticated by short tandem repeat of profiling each year. Cells were tested for *Mycoplasma* contamination routinely and confirmed negative before use. Protocol for cell line manipulations is shown in "Lentivirus-mediated expression."

FACS

Using a BD Influx flow cytometer, immune cell populations were selected by flow-cytometric cell sorting (FACS). Before cell sorting, primary cells were resuspended in PBS containing 1% FBS and incubated with Fixable Viability Dye (eBioscience, #65-0865-18) and fluorescent-linked antibodies for 30 minutes at 4°C. Pentamers were stained prior to the antibodies for 10 minutes at room temperature. To isolate CD45$^+$CD14$^+$ and CD45$^+$CD14$^-$ immune cells for single-cell RNA-seq (scRNA-seq), fluorescent-linked antibodies against CD45 (BioLegend, #982304) and CD14 (BioLegend, #367104) were used (Supplementary Fig. S1B). MUC1 pentamer (Proimmune, #F208-2A-G) and primary antibodies against CD3 (BioLegend, #317321), CD8 (BioLegend, #344718), CD161 (BioLegend, #339906), CD56 (BioLegend, #362503), Vα7.2 (BioLegend, #351707), and Vα24 (BioLegend, #342907) were used to purify CD161$^+$ and CD161$^-$ pentamer$^+$ T cells. To separate CD161$^+$ CTLs from periphery blood or TIL expansions, fluorescent-linked antibodies against CD3 (BioLegend, #317321), CD8 (BioLegend, #344718), CD161 (BioLegend, # 339906), CD56 (BioLegend, #362503), Vα7.2 (BioLegend, #351712), and Vα24 (BioLegend, #360004) were used. The purity of the sorted populations was verified by flow cytometry.

scRNA-seq

CD45$^+$ immune cells from tumor-cell suspensions of breast cancer patients in the discovery cohort were isolated through FACS. CD14$^+$ and CD14$^-$ counterparts were mixed at a ratio of 3:2 for each patient in RNase-free tubes. At least 5,000 cells were collected per patient and cells from 5 patients with the same chemotherapeutic efficacy were mixed as a sequencing sample. The cells were then resuspended at approximately 20,000 cells/mL with a final viability of > 90% as determined by flow cytometry.

Single-cell capture, lysis, cDNA library construction, generation of gel beads in emulsion (GEM), barcoding, post GEM-reverse transcription cleanup and cDNA amplification were performed using the Chromium system from 10X Genomics, with the following kits: Chromium Single-Cell 3′ Library and Gel Bead Kit v2 kit (10X Genomics, # 120237) and Chromium Single-Cell A Chip Kits (10X Genomics, #1000009). Briefly, cell suspensions were loaded on a 10X Genomics GemCode Single-cell instrument that generates single-cell Gel Bead-In-EMlusion (GEM), upon dissolution of the Gel Bead in a GEM, primers containing (i) an Illumina R1 sequence (read 1 sequencing primer), (ii) a 16-nt 10× barcode, (iii) a 10-nt Unique Molecular Identifier (UMI), and (iv) a poly-dT primer sequence were released and mixed with cell lysate and Master Mix. Barcoded full-length cDNAs were then reverse-transcribed from poly-adenylated mRNA. Silane magnetic beads were used to remove leftover biochemical reagents and primers from the post GEM reaction mixture. Full-length barcoded cDNAs were then amplified by PCR to generate sufficient mass for library construction. R1 (read 1 primer sequence) was added to the molecules during GEM incubation. P5, P7, a sample index, and R2 (read 2 primer sequence) were added during library construction via end repair, A-tailing, adaptor ligation, and PCR. Amplified cDNA was purified using SPRIselect beads (Beckman Coulter, #B23317) and sheared to 250 to 400 bp. Qualification was performed using Qubit 3.0 Fluorometer. Libraries were sequenced on an Illumina NovaSeq 6000 system, the single-cell 5′ 16-bp 10× barcode and 10-bp UMI were encoded in read 1, whereas read 2 was used to sequence the cDNA fragment. Sample index sequences were incorporated as the i7 index read. Read 1 and read 2 were standard Illumina sequencing primer sites used in paired-end sequencing. 10X Genomics Cell Ranger software (version 3.0.2) was used to convert raw BCL files to FASTQ files, and for alignment and quantification. Briefly, reads with low-quality barcodes and UMIs were filtered out and then mapped to the reference genome. Reads uniquely mapped to the transcriptome and intersecting an exon at least 50% were considered for UMI counting. The cell-by-gene matrices were produced via UMI counting and cell barcodes calling. The cell-by-gene matrices for each sample were individually imported to Seurat version 2.2.1 for downstream analysis. Cells with an unusual number of UMIs (≥20,000 or ≤600) or high mitochondrial gene percent (≥5%) were filtered out. We also excluded cells with fewer than 300 or more than 4,000 genes detected. Additionally, doublet GEMs also should be filtered out. It was achieved by using the tool DoubletFinder (v2.0.3) by the generation of artificial doublets, using the PC distance to find each cell's proportion of artificial k nearest neighbors (pANN) and ranking them according to the expected number of doublets. After removing unwanted cells from the data set, we used a global-scaling normalization method "LogNormalize" that normalizes the gene-expression measurements for each cell by the total expression, multiplies this by a scale factor (10,000 by default), and log-transforms the results. The raw data have been deposited in NCBI's Sequence Read Archive (SRA) database and are accessible through accession number PRJNA890914.
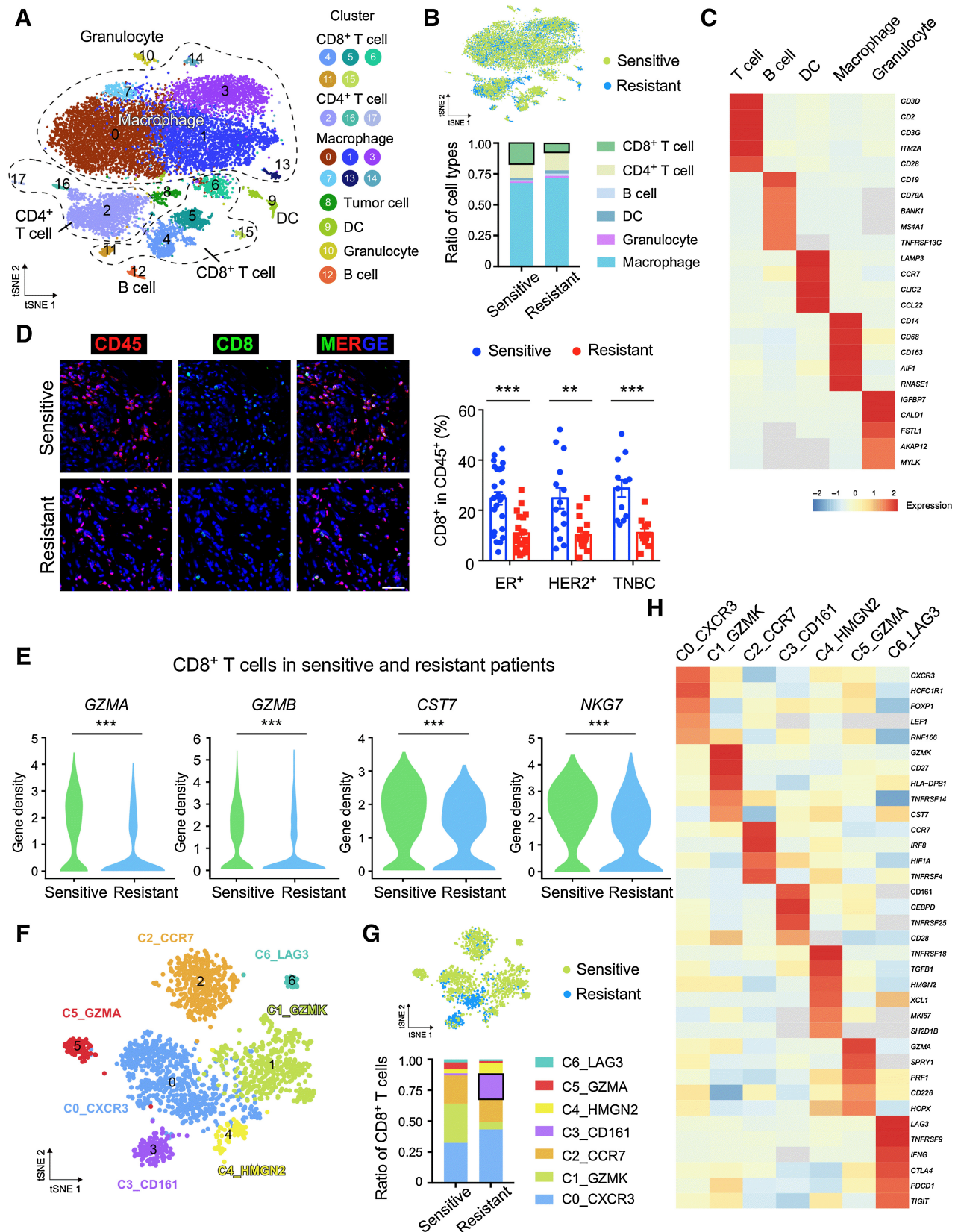
scRNA-seq data processing

Preprocessing of raw data from our study was initially performed using the Cell Ranger software pipeline (version 3.0.2). The resulting fastq files were passed to CellRanger's count, which aligned all reads against the GRCh38 genome using the STAR aligner. For each sample, the gene–barcode matrix was passed through the R (v3.5.3) software package Seurat (v2.2.1; ref. 13). We set up conservative cutoffs according to the number of genes/cell (>300) and the percentage of mitochondrial UMI counts (<5%) for quality control. Integration of the scRNA-seq data was done using Seurat functions FindIntegrationAnchors and IntegrateData after library-size normalization of each cell using NormalizeData function with default parameters. The cells were clustered using FindClusters in Seurat. T-distributed stochastic neighbor embedding (t-SNE) and modularity heat maps were created for graph-based cluster identification and subsequent dimensionality reduction. Marker genes for the individual clusters were identified using Seurat's FindAllMarkers.

Preprocessing of scRNA-seq data of 26 treatment-naïve breast cancers from the GEO data set GSE176078 (14) was performed using R software package Seurat. After integration of the scRNA-seq data and unsupervised clustering of the cells based on the condition Wu SZ and colleagues used (14), we reclustered the CD8^{+} T cells and visualized the expression profiles of specific genes by t-SNE. Patients were grouped according to CD161 expression in CD8^{+} T cells. The lymphocyte activation score of each patient was evaluated with the AddModuleScore function built in the Seurat R package according to the gene set 'GOBP_LYMPHOCYTE_ACTIVATION' (15). Then the cells labeled as "T cells CD8" were selected and divided into "CD161^{high} donors," "CD161^{low} donors," and "indefinable donors" groups according to the rate of CD161^{+} cells/CD8^{+} T cells in each patient. To explore differences in the lymphocyte activation score between the "CD161^{high} donors" and "CD161^{low} donors" groups, gene set enrichment analysis (GSEA) was conducted by the clusterProfiler package in R software. First, the differential analysis of all genes between the two groups was generated, and these genes were ordered by the value of log2 fold change. Then GSEA was performed to investigate the lymphocyte activation score correlated with different subgroups. Gene sets with $P < 0.05$ and FDR < 0.25 were considered significant.

Bulk RNA-seq

Bulk RNA-seq was performed on CD8^{+} TILs isolated from 18 breast cancer patients (6 ER^{+}, 6 HER2^{+}, and 6 TNBC patients) with different responses to chemotherapy (validation cohort 1). Purity of isolated cells was confirmed by flow-cytometric analysis before sequencing (>95%; Supplementary Fig. S1I). Total RNA was extracted from the CD8^{+} TILs using TRIzol Reagent (Thermo Fisher Scientific, # A33251) and mRNA was enriched by Oligo(dT) beads following the manufacturer's instructions. NanoDrop ND-2000 spectrophotometer was used to assess the quality of extracted RNA. Then we prepared the RNA library with total RNA as previously described (16). Briefly, the enriched mRNA was fragmented into short fragments using fragmentation buffer and reversely transcribed into cDNA by using NEBNext Ultra RNA Library Prep Kit for Illumina (New England Biolabs, # 7530). The purified double-stranded cDNA fragments were end repaired, A base added, and ligated to Illumina sequencing adapters. The ligation reaction was purified with the AMPure XP Beads (1.0X), and PCR was amplified. The resulting cDNA library was sequenced using Illumina Novaseq6000 by Gene Denovo Biotechnology Co. Reads obtained from the sequencing machines were further filtered by fastp (version 0.18.0) to get high-quality clean reads. Short reads alignment tool Bowtie2 (version 2.2.8) was used for mapping reads to the ribosome RNA (rRNA) database, the rRNA mapped reads then were removed. The remaining paired-end clean reads were mapped to the reference genome using HISAT2.2.4. The mapped reads of each sample were assembled by using StringTie v1.3.1 in a reference-based approach. For each transcription region, a fragment per kilobase of transcript per million mapped reads (FPKM) value was calculated to quantify its expression abundance and variations, using RSEM software. The raw data have been deposited in NCBI's SRA database and are accessible through accession number PRJNA890913.

Flow cytometry

For the detection of specific markers, cells from tumor digestions, peripheral blood, or TIL expansions (see "Tumor-specific T-cell expansion from tumor specimens") were suspended in PBS containing 1% FBS and 2 mmol/L EDTA and treated with FcR blocking reagent (Miltenyi Biotec, #130-059-901). Live/Dead Fixable Viability Dye-eFluor780 (eBioscience, #65-0865-18) or Zombie Aqua Fixable Viability Kit (BioLegend, #423101) was used to distinguish live cells. The fluorescent-linked antibodies were as follows: CD45 (BioLegend, #982304), CD14 (BioLegend, #367104), CD3 (BioLegend, #317314 and 317321), CD56 (BioLegend, #362512), CD8 (BioLegend, #344722, 344718, and 344724), CD161 (BD Biosciences, #562615; BioLegend, #339906), Vα7.2 (BioLegend, #351712), Vα24 (BioLegend, #360004), CD45RA (BioLegend, #983002), CD45RO (BioLegend, #983102), CCR7 (BioLegend, #353213), CD62 L (BioLegend, #304840), CD69 (BioLegend, #310905), CD103 (BioLegend, #350215), CD4 (BioLegend, #317416), IL17 (BioLegend, #512305), PD-1 (BioLegend, #135215), CTLA-4 (BioLegend, #349905), TIM-3 (BioLegend, #345005), LAG-3 (BioLegend, #369311), TIGIT (BioLegend, #372714), ICOS (eBioscience, #35-9948-41), 4-1BB (BioLegend, #309817), DR3 (BioLegend, #307105), IFNγ (eBioscience, #12-7319-42), perforin (eBioscience, #48-9994-42), granzyme B (BioLegend, #372204), CD107a (BioLegend, #328620), CD38 (BioLegend, #303506), EpCAM (BioLegend, #324214), CLEC2D (R&D Systems, #FAB3480P), HLA-A2 (BioLegend, #343304), Ki67 (BioLegend, #151210), MUC1 pentamer (Proimmune, #F208-2A-G), HER2 pentamer (Proimmune, #F214-2A-G), NY-ESO-1 pentamer (Proimmune, #F049-2A-G), HLA-A*02:01-negative control pentamer (Proimmune, #FN01-2A-G). Intranuclear staining was performed with True-Nuclear Transcription Factor Buffer Set (BioLegend, #424401), and intracellular staining was performed using an Intracellular Fixation and Permeabilization kit (eBioscience, #88-8824) according to the manufacturers' instructions.

Figure 1.

Landscape of tumor-infiltrating immune cells in chemosensitive and chemoresistant patients. Single-cell transcriptomic analysis was performed on the intratumoral immune cells of 5 chemosensitive and 5 chemoresistant breast cancer patients. **A,** t-SNE visualization of 16,152 immune cells in 5 chemosensitive and 5 chemoresistant breast cancers. **B,** t-SNE plot colored by chemosensitivity (upper) and the proportions of different types of cells in sensitive and resistant patients (lower). **C,** Heat map displaying a scaled expression of key genes for each cell type. **D,** Representative immunofluorescence images of CD45 and CD8 in chemosensitive or resistant tumors. Scale bar, 50 μm. Right, quantification stratified by subtypes (mean ± SEM; $n = 45$ for ER^{+}, $n = 32$ for HER2^{+} and $n = 23$ for TNBC). **E,** Violin plots indicating the expression of cytotoxic genes in CD8^{+} TILs of chemosensitive or chemoresistant patients. **F,** t-SNE plot of CD8^{+} T cells colored by clusters. **G,** t-SNE plot of CD8^{+} T cells colored by chemosensitivity (upper) and the fractions of different CD8^{+} T-cell subclusters in chemosensitive and chemoresistant patients (lower). **H,** Heat map displaying the expression of discriminating genes for each subcluster of CD8^{+} T cells. **, $P < 0.01$; ***, $P < 0.001$ by Student t test (**D, E**).

For intracellular cytokine staining of tumor-specific T cells, cells were restimulated *in vitro* with autologous tumor cells, NY-ESO-1$^+$ CLEC2D$^+$ MCF-7 cells, or PDX-derived tumor cells at an effector/target ratio of 1:1 for 16 hours. In the last 4 hours, brefeldin A (BioLegend, # 420601) was applied to the coculture. In some experiments, propidium iodide (# 00-6990-50, eBioscience) was used to detect the death of tumor cells. After that, flow cytometry analysis was performed immediately using Attune NxT flow cytometry analyzer instrument (Invitrogen, A24858). Data were analyzed by FlowJo software (version 10).

Immunofluorescence

For the immunostaining of paraffin sections (see "Patients and samples" for paraffin specimen collection), samples were deparaffinized first, and then antigen retrieval was performed in 0.01M citrate buffer (pH 6.0) or EDTA buffer (pH 8.0). For the immunostaining of cultured cells, cells were fixed with paraformaldehyde and then permeabilized by 0.1% Triton X-100 on ice for 15 minutes. Nonspecific antigen epitope blocking was performed using phosphate buffer containing 5% BSA for 1 hour. After that, sections or cells were probed with specific primary antibodies overnight at 4°C. The primary antibodies used were: mouse-anti-human CD8 (Abcam, #ab17147, 1:100), rabbit-anti-human CD45 (Abcam, #ab10558, 1:100), rat-anti-human CD3 (Abcam, #ab11089, 1:100), rabbit-anti-human CD161 (Abcam, #ab259916, 1:50), mouse-anti-human Vα7.2 (BioLegend, #351702, 1:50), mouse-anti-human Vα24 (BioLegend, #342902, 1:50), rabbit-anti-human EpCAM (Abcam, #ab223582, 1:500), MUC1 pentamer (Proimmune, #F208-2A-G, 1:5), HER2 pentamer (Proimmune, # F214–2A-G, 1:5), HLA-A*02:01-negative control pentamer (Proimmune, #FN01-2A-G, 1:5), rabbit-anti-human ASM (Abcam, #ab227966, 1:100), rabbit-anti-human IFNγ (Abcam, #ab231036, 1:500), and rabbit-anti-human granzyme B (Abcam, #ab134933, 1:100). Binding of antibody to antigen was visualized using Alexa Fluor 488 donkey anti-mouse secondary antibody (Invitrogen, # A21202, 1:200), Alexa Fluor 555 donkey anti-mouse secondary antibody (Invitrogen, #A31570, 1:200), Alexa Fluor 488 donkey anti-rabbit secondary antibody (Invitrogen, #A21206, 1:200), Alexa Fluor 555 donkey anti-rabbit secondary antibody (Invitrogen, #A32794, 1:200), Alexa Fluor 647 donkey anti-rabbit secondary antibody (Invitrogen, #A31573, 1:200), Alexa Fluor 488 goat anti-rat secondary antibody (Invitrogen, # A11006, 1:200), and Alexa Fluor 555 goat anti-rat secondary antibody (Invitrogen, #A21434, 1:200). For multiplex immunofluorescent staining, Opal 4-color manual IHC kit (PerkinElmer, #NEL840001KT) was used according to the manufacturer's instructions. DAPI (Thermo Fisher Scientific, # D3571) was used for nuclei counterstaining, and laser-scanning confocal microscopy (Zeiss, LSM780) was used for imaging. In the representative immunofluorescent images, asterisks denote the area of higher magnification images.

Primary cell isolation from peripheral blood

Peripheral blood mononuclear cells were isolated by Ficoll density gradient centrifugation from blood samples from breast cancer patients or healthy donors from the Guangzhou Blood Center. Briefly, blood samples diluted 1:1 with PBS were gently layered over Ficoll-Paque PLUS (TBDscience, #LTS1077). After centrifugation at $450 \times g$ for 20 minutes with the brake off (Beckman, X-15R), mononuclear cells were collected from the interface, washed 3 times with PBS and resuspended in DMEM. After 20 minutes of incubation at 37°C, the nonadherent cells (periphery blood lymphocytes) were removed to acquire mono-

cytes. Monocyte-derived dendritic cells (mo-DC) were generated by culturing monocytes with 20 ng/mL IL4 (PeproTech, # 200-04-20) and 50 ng/mL GM-CSF (PeproTech, # 300-03-20) for 6 days. CD8$^+$ T cells and natural killer (NK) cells were isolated by magnetic-activated cell sorting using direct CD8 and CD56 Isolation Kits (Miltenyi Biotec, #130-094-156 and 130-050-401) according to the manufacturer's instructions. CD8$^+$ T cells and NK cells were cultured in RPMI-1640 medium supplemented with 25 mmol/L HEPES (Thermo, # 15630080), 4 mmol/L L-glutamine (Thermo, # A2916801), 25 μmol/L 2-mercaptoethanol (Thermo, # 21985023), and 10% FBS. Media were replaced every 2 days.

Tumor-specific T-cell expansion from tumor specimens

Tumor-specific T cells were generated from tumor specimens with a well-established two-step method, as described previously (17, 18). During the initial outgrowth [pre–rapid expansion protocol (REP)], single-cell suspensions of digested primary breast tumor tissue generated as aforementioned (see "Primary cell isolation from tumor tissue") were cultured in RPMI-1640 medium supplemented with 10% FBS and 6000 IU/mL of IL2 (Novartis) to allow TIL outgrowth for 14 to 21 days. In some experiments, CD161$^+$ CTLs were isolated via FACS and edited by Cas9 protein with control or CD161 gRNA (see "CRISPR-mediated gene knockout"). In the second step, cells were further expanded using a standard small-scale REP with irradiated allogeneic feeder cells (40 Gy, 200:1), CD3 antibody (Miltenyi Biotec, #130-093-387, clone OKT3, 30 ng/mL), and 6,000 IU/mL of IL2. Periphery blood lymphocytes from healthy donors were irradiated (Rad Source, Rs2000) and served as feeder cells. One cycle of REP (14 days) resulted in massive T-cell expansion.

Lentivirus-mediated expression

Human T cells freshly isolated from peripheral blood were infected with recombinant lentiviral particles for CD161 or NY-ESO-1 TCR (the TCR recognizing the NY-ESO-1:157–165 epitope presented by HLA-A*02:01) and MCF-7 cells were infected with lentiviral expression vectors for NY-ESO-1 or CLEC2D with 8 μg/mL polybrene (Biosharp, # BL628A) overnight at 37°C. The transduced cells were selected with 2.5 μg/mL puromycin (Asegene, # 43137) for 2 weeks to obtain the CD161/NY-ESO-1 TCR-expressing T cells and NY-ESO-1/CLEC2D-expressing MCF-7 cells, respectively. Lentivirus packaging was provided by GenePharma Inc using LV3/LV5 lentiviral vectors. The sequences of NY-ESO-1-TCRα and NY-ESO-1-TCRβ were as we previously described (19).

Western blot analysis

Western blot analysis was performed to assess the expression of the proteins of interest using standard procedures. Briefly, lentivirus-treated cells or cells isolated from tumor suspensions were lysed by RIPA (Millipore, # 20-188) with protease and phosphatase inhibitor (Thermo Fisher Scientific, #78444), protein concentration was measured by a Pierce BCA Protein Assay kit (Thermo Fisher Scientific, #23225). Equal protein amounts were resolved by 10% SDS-PAGE and then blotted onto PVDF membranes. After blocking by 5% BSA, PVDF membranes were incubated with primary antibodies at 4°C overnight and then secondary antibody for 1 hour at room temperature. The primary antibodies used were: anti-CLEC2D (Abcam, #ab151738, 1:1,000), anti-ASM (Abcam, # ab227966, 1:1,000), anti-CD161 (BD, # 940283, 1:50), anti-NY-ESO-1 (Proteintech, #19521-1-AP, 1:1,000), and anti-GAPDH (Proteintech, #HRP-60004, 1:10,000). The secondary antibodies used were: HRP-linked anti-rabbit antibody (Cell Signaling Technology, #7074, 1:3,000), HRP-linked anti-mouse

antibody (Cell Signaling Technology, #7076, 1:3,000), and HRP-linked anti-rat antibody (Cell Signaling Technology, # 7077, 1:3,000). Signals were detected by chemiluminescence (Thermo Fisher Scientific, # 34580).

In situ hybridization

In situ RNA hybridization was performed using the RNAscope Multiplex Fluorescent Reagent Kit (Advanced Cell Diagnostics, #323100) following the manufacturer's protocol. Briefly, deparaffinized
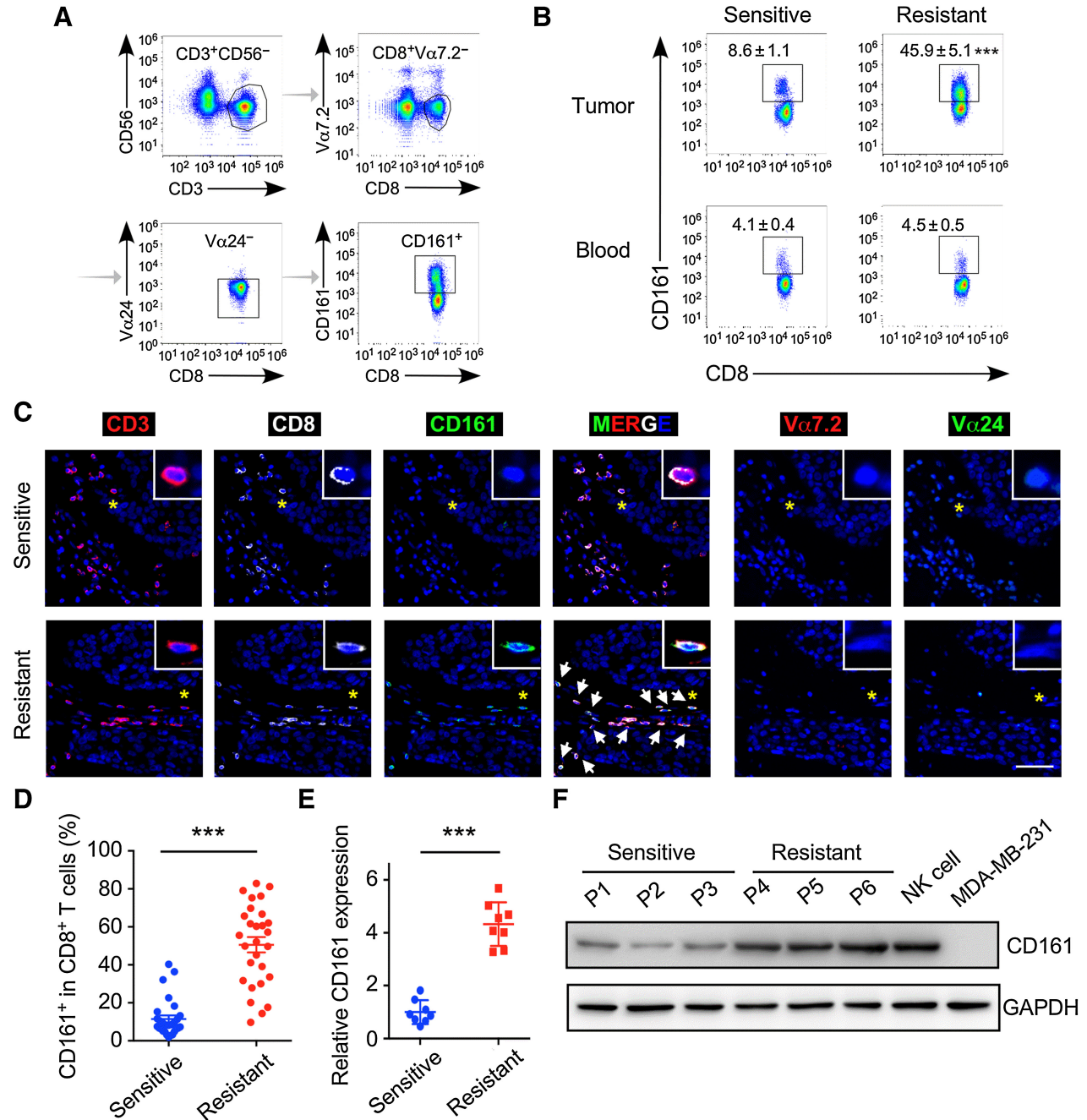
Figure 2.
The CD161+CD8+ T-cell subset is enriched in chemoresistant tumors. CD161 expression was examined in tumor-infiltrating CD8+ T cells of tumor suspensions or paraffin sections from pretreatment biopsies of breast cancer patients. **A,** Representative gating strategy for flow cytometry of CD161+ CTLs. Vα7.2 was used to exclude MAIT cells and Vα24 to exclude NKT cells. **B,** Representative flow cytometry of CD161 expression gated as **A** in paired tumor samples and peripheral blood ($n = 24$ different patients). See stratified quantification in Supplementary Fig. S2E. **C** and **D,** Representative immunofluorescence images (**C**) and quantification (**D**) for CD3, CD8, CD161, Vα7.2, and Vα24 in serial sections of breast cancer biopsies ($n = 28$ different patients). Arrows indicate CD161+ CTLs. Scale bar, 50 μm. **E** and **F,** Quantitative RT-PCR (**E**) and representative western blot (**F**) for CD161 expression in FACS-isolated conventional CD8+ T cells from tumor suspensions ($n = 8$ different patients for **E** and 3 for **F**). See quantification of **F** in Supplementary Fig. S2G. Results are mean $\pm$ SEM. ***, $P < 0.001$ by Student t test (**B**–**E**).
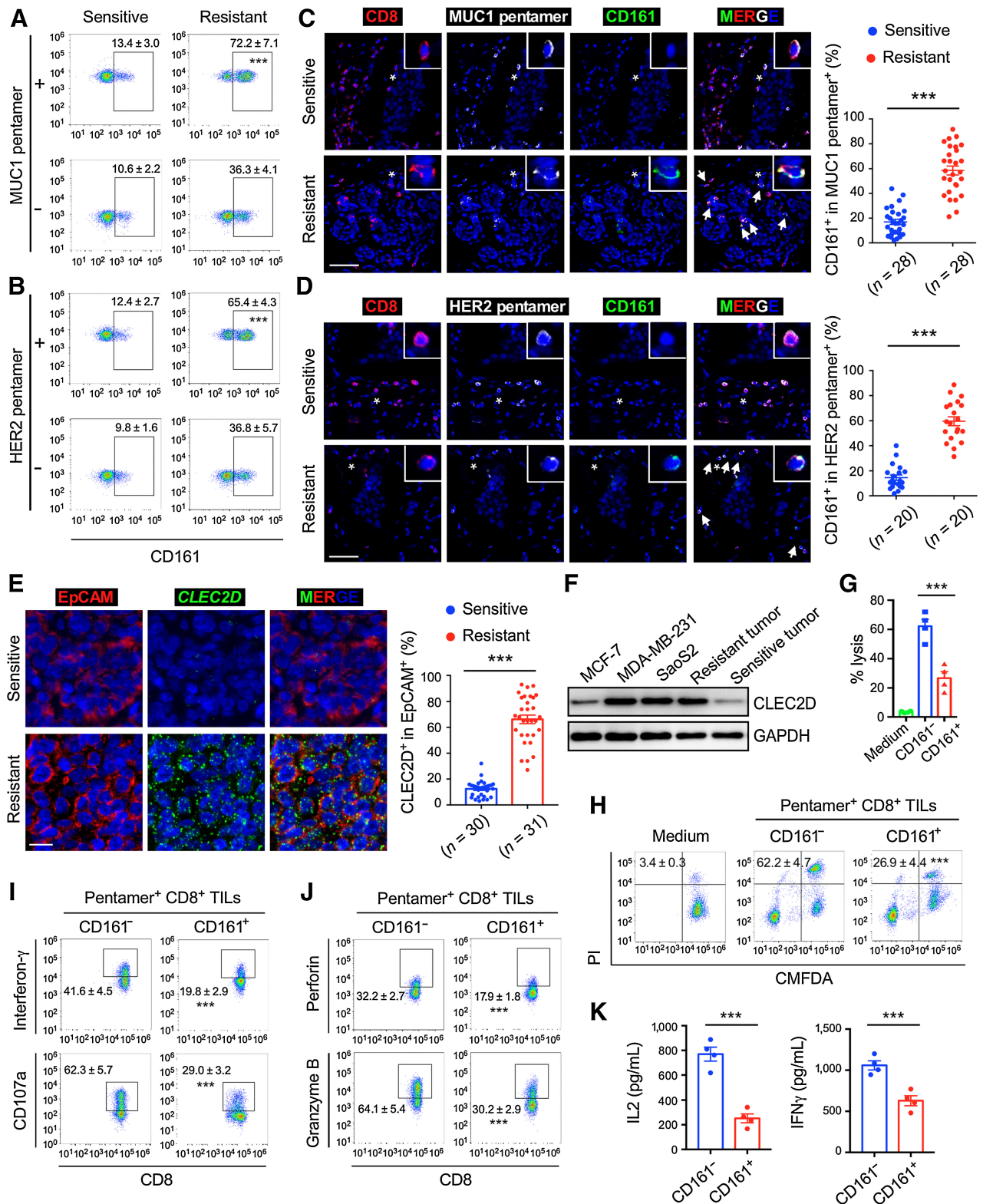
sections of breast cancer patients obtained via large core-needle biopsy before neoadjuvant chemotherapy were first treated with RNAscope Hydrogen Peroxide, and then antigen retrieval was performed in RNAscope Target Retrieval Reagent. Hs-NPM1-X-*CLEC2D* (Advanced Cell Diagnostics, #419751) probes were added to the tissue and hybridized for 2 hours at 40°C. A series of signal amplification steps were performed using RNAscope Multiplex Fluorescent Reagent Kit. After that, the EpCAM immunostaining and nuclei counterstaining were performed as described before (see "Immunofluorescence"). Finally, sections were cover-slipped for examination on a Zeiss LSM780 confocal microscope.

IHC

Paraffin sections of tissue samples obtained from reduction mammaplasties, breast cancer biopsies, breast tumor resections, or patient-derived xenografts (PDX; see "PDX implantation") were deparaffinized first and then antigen retrieval was performed in 0.01M citrate buffer (pH 6.0) or EDTA buffer (pH 8.0). After 3% hydrogen peroxide treatment and blocking, a primary antibody for MUC1 (Abcam, #ab45167, 1:500), HER2 (Abcam, #ab134182, 1:300), ERα (Abcam, #ab32063, 1:200), or PR (Abcam, #ab32085, 1:100) was incubated overnight at 4°C and the signaling was amplified via incubation for 1 hour at room temperature with HRP-conjugated secondary antibodies from an anti-mouse/rabbit IHC Secondary Antibody Kit (Dako, # GK500710). After washing, DAB peroxidase substrate (Dako, # GK500710) was dropped on top of the slides and visualized under a microscope (Olympus, BX-63) for brown staining. The reaction was stopped by dipping slides into a large amount of PBS. Images were taken with Olympus BX-63 microscope.

qRT-PCR

Total RNA was extracted from isolated T cells by using the CellAmp Direct RNA Prep Kit for RT-PCR KIT (TaKaRa, # 3732). For each sample, 100 μg of total RNA was reversely transcribed into cDNA using PrimeScript RT Master Mix (TaKaRa, # RR036A). And then quantitative PCR was performed using SYBR Premix Ex Taq kit (TaKaRa, # RR820A) according to the manufacturer's instructions. At least three replicates were included in each analysis. Data were collected and analyzed with a LightCycler 480 instrument (Roche). GADPH was used for normalization and relative gene expression was determined by the $2^{-\Delta\Delta CT}$ method. The primer sequences were listed in Supplementary Table S1.

Generation of tumor-specific DCs and T cells

To generate antigen-specific DCs, mo-DCs, generated as described in "Primary cell isolation from peripheral blood," were matured through incubation with 100 ng/mL LPS (Invitrogen, # 00-4976-93) and 500 U/mL IFNγ (PeproTech, # 300-02) for 48 hours and then pulsed for 24 hours with cancer cell lysates generated by five freeze–thaw cycles (200 μg protein/1 × 10⁶ cells/mL) from autologous tumor cells. To generate tumor-specific CTLs, we incubated CD8⁺ T cells with antigen-specific DCs (5:1) for 6 days.

ELISA

Primary tumor cells, NY-ESO-1⁺ CLEC2D⁺ MCF-7 cells, or tumor cells isolated from PDXs were seeded in triplicate into 96-well plates prior to the addition of autologous CD161⁺ CTLs, ESO CTLs (CD161⁺ CTLs isolated from peripheral blood of healthy donors and introduced with an NY-ESO-1—specific TCR) or CD161⁺ CTLs for adoptive transfer (see "Adoptive T-cell transfer therapy") at an effector/target ratio of 1:1. After 72 hours, the supernatants were collected by centrifugation for subsequent ELISA detection. IL2 and IFNγ human ELISA kits (Thermo Fisher Scientific, #BMS221-2, KHC4021) were used according to the manufacturer's instructions. For some experiments, CD161-blocking mAb (BioLegend, #339902) or mouse IgG control Ab (BioLegend, # 401402) was added to the coculture at a final concentration of 10 μg/mL. The OD values were measured with a Mithras microplate reader (Berthold, LB 940).

Cytotoxicity of CD8⁺ T cells

To assess the cytotoxicity of ESO CTLs, MCF-7 breast cancer cells were transduced with NY-ESO-1 and CLEC2D lentiviral vectors (NY-ESO-1⁺ CLEC2D⁺ MCF-7). NY-ESO-1⁺CLEC2D⁺ MCF-7 cells were labeled by CellTracker CMFDA Dye (Thermo Fisher Scientific, #C7025) and passed through Dead Cell Removal Microbeads (Miltenyi Biotec, #130-090-101), then cocultured with ESO CTLs at an effector/target ratio of 1:1 for 8 hours. For the cytotoxicity of TILs, primary breast cancer cells were isolated from tumor tissue and purified by EpCAM Microbeads (Miltenyi Biotec, #130-061-101). Then cell-tracker-labeled primary tumor cells were passed through Dead Cell Removal Microbeads and cocultured with autologous pentamer⁺ CTLs (CTLs isolated by FACS using MUC1 pentamer) at an effector/target ratio of 1:1 and autologous CD161⁺ CTLs at an effector/target ratio of 10:1 for 12 hours. In some experiments, CD161⁺ and CD161⁻ T cells were separated and seeded into 96-well plates via FACS (BD Influx). At the end of the coculture, all cells were stained with PI (eBioscience, # 00-6990, 1:50) and analyzed by flow cytometry immediately. In some experiments, T cells were preincubated with imipramine (Sigma-Aldrich, #I0899, 100 μmol/L) for 1 hour before coculturing with autologous tumor cells.

CRISPR-mediated gene knockout

CRISPR-mediated gene knockout was performed as we previously described (20). The sequences targeting *CD161* were *CD161* gRNA1 (5′-AATTAAAGCCACTTACCCCG-3′) and *CD161* gRNA2 (5′-TTACCCCGAGGAAGAGATGA-3′). Freshly isolated human T cells

---

Figure 3.
CD161 is preferentially expressed in tumor-specific CD8⁺ T cells and associated with compromised T-cell cytotoxicity. Tumor-specific CD8⁺ T cells of HLA-A*02:01 breast cancer patients, determined by pentamer staining, were detected for CD161 expression. Then CD161⁺ and CD161⁻ pentamer⁺ CTLs were purified and analyzed for their antitumor capacity. **A** and **B,** Flow cytometry for CD161 in pentamer⁺ and pentamer⁻ CTLs from chemosensitive and resistant tumors ($n = 8$ different patients). **C** and **D,** Representative immunofluorescent images and quantification for CD161 expression in pentamer⁺ CTLs of chemosensitive and resistant tumors ($n = 28$ different patients for **C** and 20 for **D**). Scale bar, 50 μm. **E,** Representative images and quantification of FISH for *CLEC2D* and immunofluorescence for EpCAM in breast cancer ($n = 30$ for sensitive group and 31 for resistant). Scale bar, 10 μm. **F,** Representative western blot for CLEC2D expression of MACS-sorted EpCAM⁺ cells from chemoresistant and chemosensitive tumors ($n = 3$). **G** and **H,** Representative plots and quantification of cytotoxicity of CD161⁺ and CD161⁻ pentamer⁺ tumor-specific CTLs from TIL expansions against autologous tumor cells ($n = 4$ different patients). **I–K,** Flow cytometry for IFNγ, CD107a (**I**), perforin, granzyme B (**J**), and ELISA for IFNγ and IL2 (**K**) of CD161⁺ and CD161⁻ pentamer⁺ CTLs from chemoresistant patients against autologous tumor cells ($n = 4$ different patients). See quantification of **I–J** in Supplementary Fig. S3K. Results are mean ± SEM. ***, $P < 0.001$ by paired Student t test compared with pentamer⁻ CTLs (**A, B**) or CD161⁻ cells (**G–K**). ***, $P < 0.001$ by an unpaired Student t test compared with chemosensitive patients (**C–E**).

---
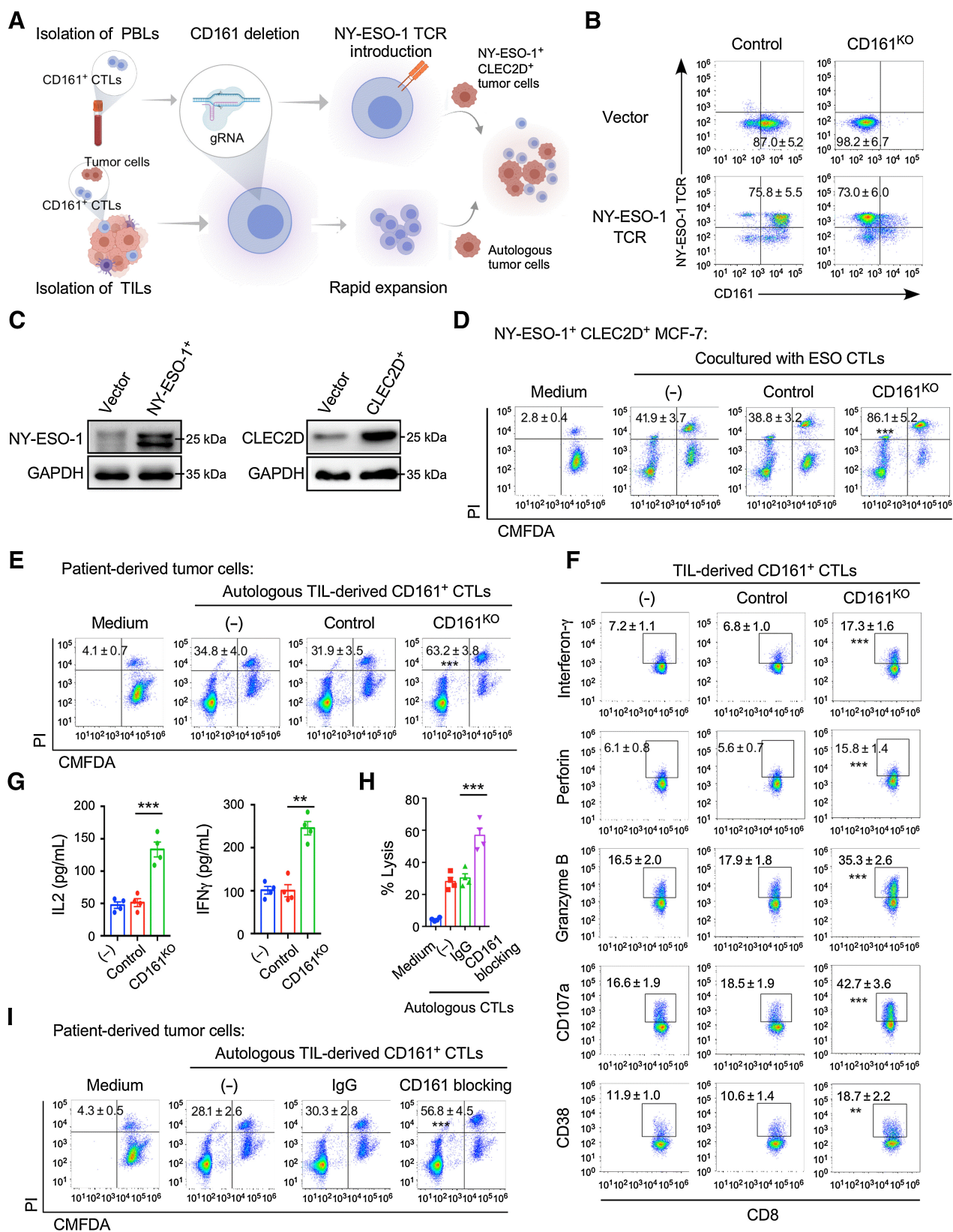
or ESO CTLs were transduced with the Cas9 lentivirus and CD161 gRNA1/2 lentivirus purchased from GenePharma. Briefly, cells were plated at 5×10^5 cells per mL in 24-well plates and transduced with lentiviral particles (MOI of 50) with 8 µg/mL polybrene (Biosharp, # BL628A) overnight at 37°C. The transduced cells were selected with 2.5 µg/mL puromycin (Asegene, # 43137) for 2 weeks to obtain the CD161 knockout T cells.

Ceramide production

T cells were lysed in lysis buffer (50 mmol/L sodium acetate [pH 5], 0.5% Nonidet P-40). 10 µg cell lysates from T cells was incubated with 0.2 mg sphingomyelin (Sigma-Aldrich, # 85615, dissolved in a 1:1 mixture of chloroform and methanol) for 2 hours and then loaded 30 µL onto a silica gel 60 thin-layer chromatography plate (EMD Millipore, #99570) along with known concentrations of ceramide (natural ceramide, APExBIO, #A4534). Then the thin-layer chromatographic separation was performed using a solvent system of chloroform and methanol (3:2) for 40 to 80 minutes until the solvent front was 1 to 2 cm from the top. Ceramide was visualized in iodine vapor and scanned by a high-resolution gel imaging system (Bio-Rad, Gel Doc XR). ImageJ software (NIH) was used to evaluate relative ceramide levels. In some experiments, T cells were preincubated with imipramine (Sigma-Aldrich, # I0899, 100 µmol/L) for 1 hour before microbead-mediated CD161 cross-linking (see "Intracellular Ca^{2+} measurements") and ceramide production measurements.

Intracellular Ca^{2+} measurements

Intracellular calcium fluxes were measured as described previously (21). Briefly, CTLs with ASM or CD161 silencing were labeled with Fura-2-AM (Beyotime, #S1052, 1 µmol/L) for 30 minutes at 37°C. For CD161 cross-linking, T cells were incubated with anti-biotin microbeads (Miltenyi Biotec, #130-092-357) loaded with biotinylated anti-CD161 antibody (Miltenyi Biotec, #130-092-906) or isotype-biotin control (BioLegend, # 400104) for 3 minutes at 37°C. Intracellular Ca^{2+} was recorded at 500 nm emission in response to 340 nm/380 nm excitation using a fluorescence spectrophotometer (RF-5000; Shimadzu). T cells were stimulated by the addition of 40 µg/mL biotinylated anti-CD3ε (Miltenyi Biotec, #130-093-377, clone OKT3) followed by 20 µg/mL streptavidin (Thermo Fisher Scientific, #434301). For flow-cytometric analysis, T cells were labeled with Fura-3-AM (Beyotime, #S1056, 1 mmol/L) and Live/Dead Fixable Viability Dye-eFluor780. Calcium fluorescence was monitored at an emission wavelength of 530 nm with excitation at 488 nm. For fluorescent microscopy imaging, cells were loaded with Furo-3-AM, Hoechst 33342 (Thermo Fisher Scientific, # 62249), and PE-conjugated anti-human CD8a antibody (BioLegend, #301008) on a confocal dish and analyzed on an LSM 780.

shRNA-mediated silencing

Lentivirus containing shRNAs against acid sphingomyelinase (ASM) were constructed by GenePharma and then used to transduce

CD161$^+$ CTLs from TIL expansions with 8 µg/mL polybrene overnight at 37°C. The transduced cells were then selected with 2.5 µg/mL puromycin for 2 weeks. The shRNA target sequences are listed as follows: human *ASM* (sh1), 5′-GTCTATTCACCGCCATCAA-3′; human *ASM* (sh2), 5′-CTACCT ACATCGGCCTTAA-3′. To rescue the expression of ASM in ASM-silenced T cells, ASM-silenced T cells were infected with recombinant lentiviral particles (LV5 lentiviral vectors carrying ASM) custom-made by GenePharma Inc.

PDX implantation

PDX implantation was performed as previously described (22). Primary tumor samples were obtained from patients with breast cancer by tumor resection at the Sun Yat-Sen Memorial Hospital from 2018 to April 2020. PDX transplantation was performed using 4-week-old female NOD-SCID mice purchased from the Jackson Laboratory and at least three mice per experimental group. All the animal experiments were performed in accordance with the ethics boards and the Clinical Research Committee at Sun Yat-Sen Memorial Hospital. All mice were maintained under defined conditions at the Animal Experiment Center of Sun Yat-Sen University. The primary breast tumor samples were minced into fragments of 1 to 2 mm^3. The skin on the abdomen of anesthetized mice was lifted, and a stainless-steel precision trochar was used to implant the tumor fragments into the inguinal mammary glands. Tumor growth was monitored every 4 days with calipers. Tumor volumes were calculated with the formula $0.5 \times \text{length} \times (\text{width})^2$. When palpable PDXs had been established, NOD-SCID mice were treated with adriamycin and cyclophosphamide (Sigma-Aldrich, #D1515 and #C0768) intraperitoneally at doses of 2 and 100 mg/kg, respectively. Two days later, autologous T cells and DCs were infused through tail-vein injection. Simultaneously and repetitively, an anti-CD161 antibody or control IgG was administered intravenously in model A, whereas IL2 was administered subcutaneously in model B (see "Adoptive T-cell transfer therapy"). Tumor volume record started from the day of cell transfer (d0) and lasted until 28 days after that (d28). On day 28, mice were harvested and PDX samples were collected for paraffin embedding and cell disassociation.

Adoptive T-cell transfer therapy

Adoptive T-cell transfer therapy was performed as previously described (23). In model A, CD8$^+$ T cells purified from patient blood were transduced with CD161-overexpression lentivirus and then cocultured with autologous mo-DCs that had been pulsed by tumor lysates as aforementioned (see "Generation of tumor-specific DCs and T cells"). 0.5×10^6 DCs and 2.5×10^6 CTLs were transferred into NOD-SCID mice that formed autologous PDXs through tail-vein injection 2 days after chemotherapy. CD161 blocking mAb (clone HP-3G10, BioLegend, # 339902) or mouse IgG control Ab (IgG1, κ Isotype, BioLegend, #401408) were intravenously injected 1 day before ACT and repeated every 3 days. In model B, CD161$^+$ CTLs were sorted from tumor-specific T cells expanded from TILs and edited with

Figure 4.
CD161 serves as an inhibitory receptor in tumor-specific CD8$^+$ T cells. CD161 was inactivated genetically or pharmaceutically in CD8$^+$ TILs expanded from cancer patients or engineered CTLs from healthy individuals before their cytolytic functions were analyzed *in vitro*. **A,** Schematic of the experimental design for two coculture models. **B,** Flow cytometry for CD161 and NY-ESO-1 TCR 3 days after CD161 inactivation and/or NY-ESO-1 TCR introduction. **C,** Western blot for NY-ESO-1 and CLEC2D in MCF-7 cells with NY-ESO-1 and CLEC2D overexpression. The data are representative of $n = 3$. **D,** Tumoricidal effects of ESO CTLs with or without CD161 inactivation against NY-ESO-1$^+$CLEC2D$^+$ MCF-7 cells. **E,** Tumoricidal effects of CD161$^+$ CTLs from TIL expansions with or without CD161 deletion against autologous tumor cells. **F** and **G,** Flow cytometry for IFNγ, perforin, granzyme B, CD107a and CD38 expression (**F**) and ELISA for IL2 and IFNγ (**G**) of TIL-derived CD161$^+$ CTLs in response to autologous tumor cells. **H** and **I,** Representative plots and quantification of tumoricidal effects of CD161$^+$ CTLs against autologous tumor cells with control IgG or CD161 blocking antibody (HP-3G10) treatment. See quantification of **C–F** in Supplementary Fig. S4E–S4H. Results are mean ± SEM of $n = 5$ (**B, D**) or 4 (**E–I**) different individuals. **, $P < 0.01$; ***, $P < 0.001$ by two-sided one-way ANOVA with the Tukey test (**D–I**).
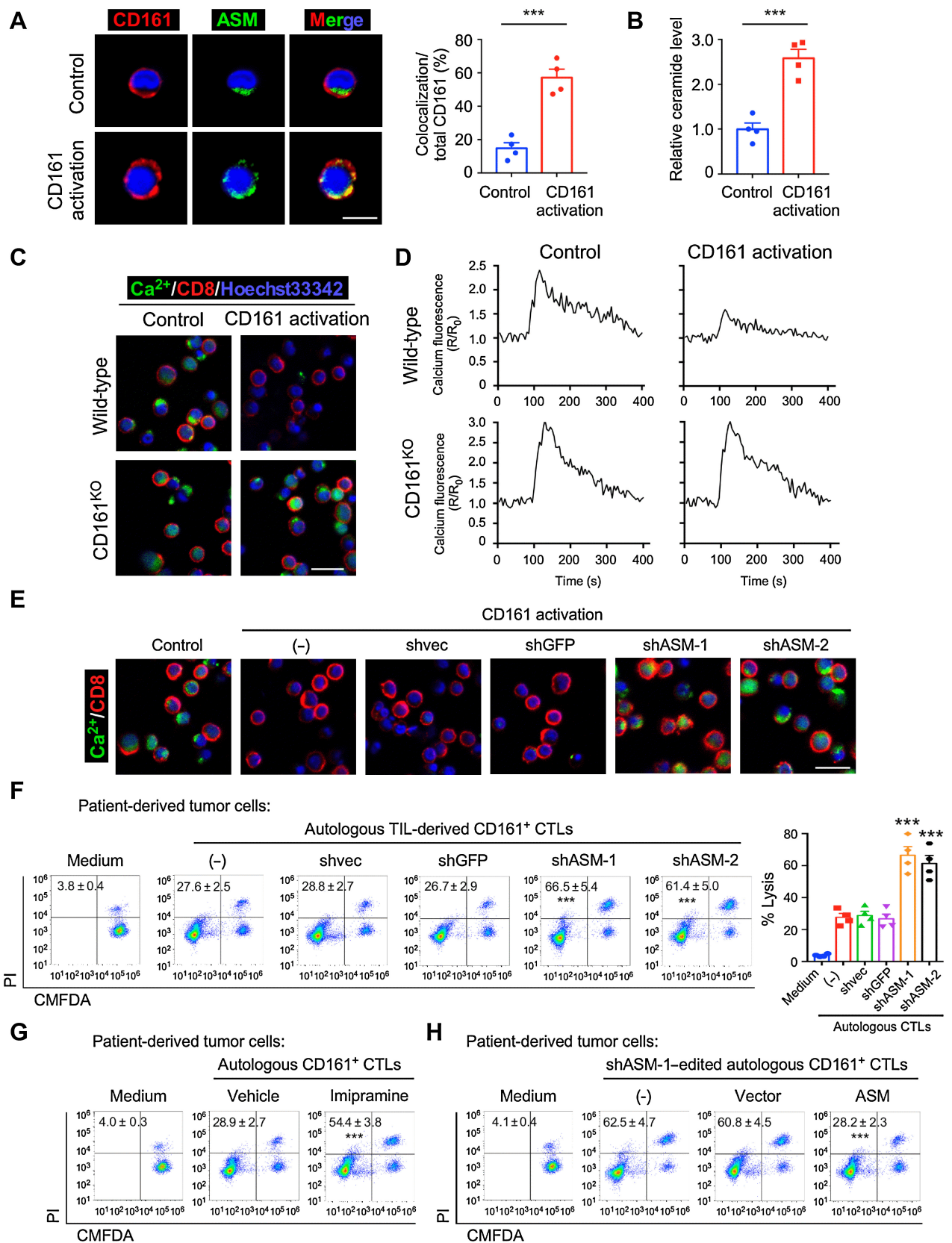
control or CD161 gRNA. 5×10^6 CTLs and 1×10^6 autologous DCs were transfused intravenously per mouse and recombinant human IL2 (45,000 IU, Novartis) was subcutaneously administrated daily after CTL transfer.

TUNEL assay

Paraffin sections of tumor samples from 535 patients in validation cohort 2 were deparaffinized first and then cell death was detected by using the In Situ Cell Death Detection Kit POD (Roche, #11684817910) according to the manufacturer's instruction. A confocal laser-scanning microscope (Carl Zeiss, LSM780) was used to scan images.

Statistical analysis

The details of statistical information are indicated in the figure legends or Materials and Methods. Unless otherwise described in the figure legends or Materials and Methods, statistical values were determined using GraphPad Prism 8.0. For quantification of immunofluorescent analysis, each data point is the mean of five fields for each patient. In validation cohort 2, numbers of CD161$^+$ CTLs and TUNEL$^+$ apoptotic tumor cells per field were quantified by ImageJ. Pearson correlation was used to assess the association between the infiltration of CD161$^+$ CTLs and TUNEL$^+$ tumor cells. For survival analysis, X-tile statistical software version 3.6.1 (Yale University School of Medicine) was applied to determine the optimal cutoff point based on the minimum P value calculated by the highest χ^2 value. Patients in validation cohort 2 were divided into two groups based on the CD161$^+$ proportions of CD3$^+$CD8$^+$ tumor-infiltrating cells (CD161$^+$% in CTLs) and according to the cutoff point by X-tile. P values for survival analysis were calculated with a two-sided log-rank test. All *in vitro* experiments were performed for at least three independent experiments and the specific numbers are indicated in the figure legends. All experiments using human samples were performed with three experimental replicates for each individual and each data point represents the mean of triplicates from each human. Some functional experiments were performed in triplicate from 3 to 5 donors and yielded similar results. Data related to PDX-bearing mice were representative of three independent experiments using 3 to 5 mice per group. Two-tailed Student t tests were used to identify significant differences between two groups and two-tailed one-way ANOVA with Dunnett test was used to determine the statistical difference in the experiments with more than two groups. All bar graphs show means and error bars (indicating SEM or SD), as mentioned in each figure legend. $P < 0.05$ was considered statistically significant.

Data availability

The sequence data generated have been deposited in NCBI's SRA database and are accessible through accession numbers PRJNA890913 (RNA-seq) and PRJNA890914 (scRNA-seq). All other data are available in the main text or the supplementary materials or are available from the corresponding author upon reasonable request. Online breast cancer scRNA-seq data were obtained from GEO: GSE176078.

Results

### Landscape of tumor-infiltrating immune cells in chemosensitive and chemoresistant patients

To dissect the tumor microenvironment of breast cancer patients with different responses to chemotherapy, we dissociated tumor specimens acquired prior to neoadjuvant chemotherapy via large core-needle biopsy from 5 patients who were subsequently determined to be chemosensitive and 5 who were subsequently determined to be chemoresistant (discovery cohort; Supplementary Fig. S1A). Detailed clinical information for these patients is listed in Supplementary Table S2. The intratumoral immune cells from each patient were purified by FACS (Supplementary Fig. S1B) and profiled by full-length scRNA-seq. After quality control filtering and outlier cell exclusion, a total of 16,152 cells were obtained for subsequent analyses, with averages of 6,400 UMIs and 1,880 genes per cell (Supplementary Fig. S1C and S1D).

Using the t-SNE method, 18 clusters of cells were visualized (**Fig. 1A**), among which stable expression of housekeeping genes was observed (Supplementary Fig. S1E). We identified 6 types of cells, including macrophages, T cells, B cells, DCs, and granulocytes (**Fig. 1A–C**; Supplementary Fig. S1F). Chemosensitive and chemoresistant patients exhibited a similar composition of intratumoral immune cell types, but the fraction of CD8$^+$ T cells in chemoresistant tumors was much lower than that in chemosensitive tumors (7.6% vs. 16.4%; **Fig. 1B**). Immunofluorescence staining for CD45 and CD8 in tumor specimens acquired prior to neoadjuvant chemotherapy via large-core needle biopsy from another cohort of 100 patients validated the reduction in CD8$^+$ T cells in chemoresistant tumors (**Fig. 1D**; Supplementary Table S3).

In further analysis, signature genes associated with T-cell cytotoxicity (*GZMA, GZMB, CST7, NKG7, PRF1,* and *CD69*) showed a weaker signal in CD8$^+$ T cells from chemoresistant patients than in those from chemosensitive ones (**Fig. 1E**; Supplementary Fig. S1G). Reclustering of CD8$^+$ T-cell subsets revealed 7 populations including C0_CXCR3, C1_GZMK, C2_CCR7, C3_CD161, C4_HMGN2, C5_GZMA, and C6_LAG3 (**Fig. 1F–H**; Supplementary Fig. S1H). In comparison with chemosensitive patients, chemoresistant patients displayed a marked reduction in cytotoxic C1_GZMK cells and a slight increase in unresponsive C0_CXCR3 cells (**Fig. 1G**). Intriguingly, a distinct subset (C3_CD161 cells) was sparse in chemosensitive patients but accounted for a considerable proportion of the CD8$^+$ TILs in chemoresistant patients (1.9% vs. 21.1%; **Fig. 1G**), suggesting that these cells may provide a clue for the processes involved in immune evasion and treatment resistance.

Figure 5.
CD161 engagement blocks calcium influx in CTLs through ASM activation and ceramide generation. **A,** Representative immunofluorescence staining for CD161 and ASM in TIL-derived CD161$^+$ CTLs treated with microbeads loaded with control IgG or CD161 cross-linking mAb (CD161 activation). Scale bar, 5 μm. Right, quantification of colocalization percentage of ASM and CD161 signals. **B,** Relative intracellular ceramide level of CD161$^+$ CTLs treated with control or CD161 stimulating microbeads. **C,** Representative fluorescent images for calcium entry of Fura-3 loaded CD161$^+$ CTLs pretreated with control or CD161 cross-linking microbeads upon TCR activation by CD3 stimulating mAb (OKT3). Scale bar, 10 μm. **D,** Representative tracings for intracellular Ca^{2+} concentrations in Fura-2–loaded CD161$^+$ CTLs pretreated with control or CD161 cross-linking microbeads and activated by CD3 mAb. **E,** Representative fluorescent images for calcium influx of CD161$^+$ CTLs edited with different shRNAs upon TCR stimulation. Scale bar, 10 μm. **F** and **G,** Tumoricidal effects of TIL-derived CD161$^+$ CTLs edited with different shRNAs (**F**) or treated with vehicle or imipramine (**G**) against autologous tumor cells. **H,** Tumoricidal effects of shASM-1–treated CD161$^+$ CTLs with or without ASM reconstitution. See the quantification of **G, H** in Supplementary Fig. S5F and S5H. Shown are representative or mean ± SEM of $n = 4$ (**A, B, F–H**) or $n = 3$ (**C–E**) different patients. ***, $P < 0.001$ by the Student t test (**A, B, G**) or two-sided one-way ANOVA with the Tukey test (**F, H**).
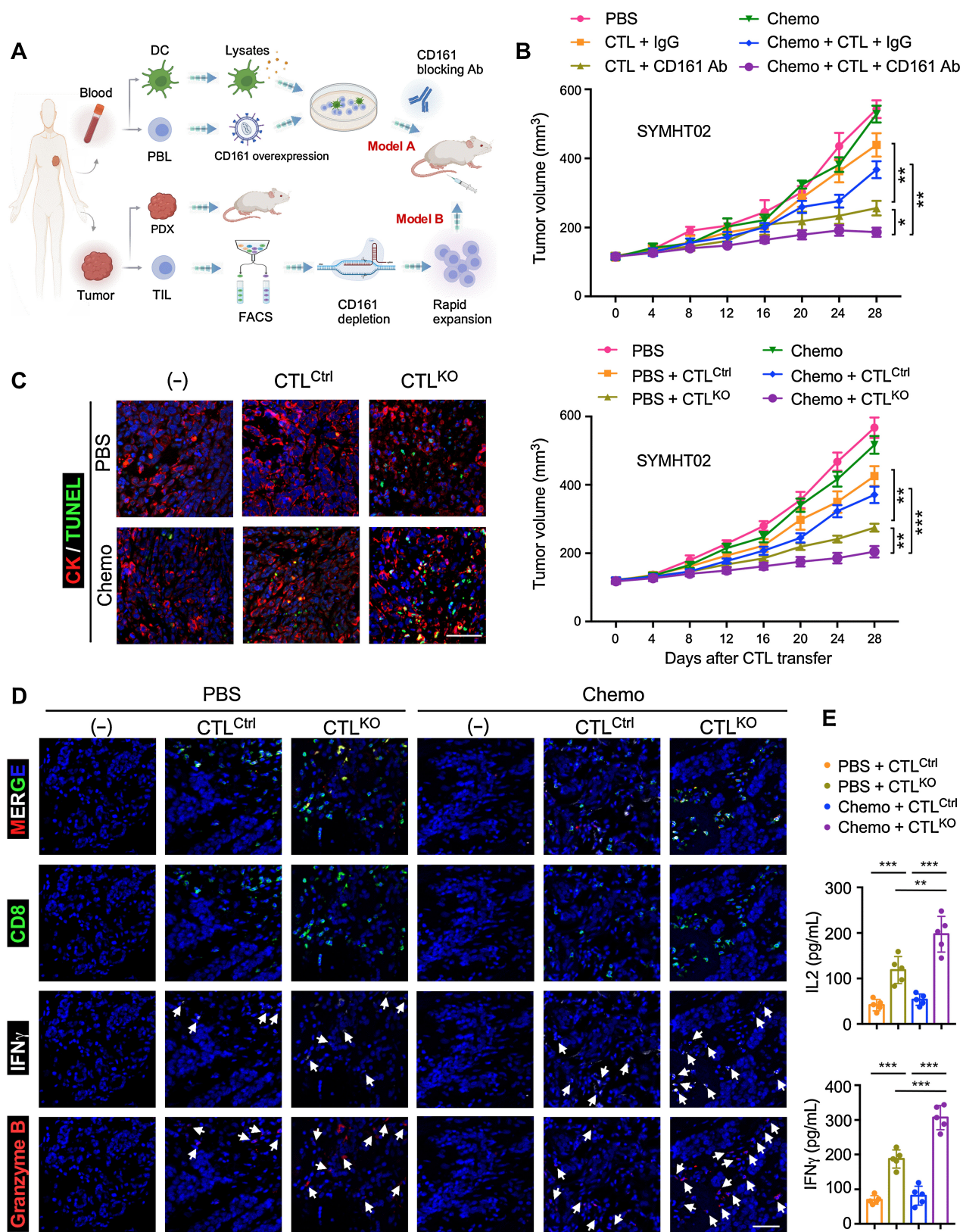
A validation cohort of 18 patients (6 ER$^+$, 6 HER2$^+$, and 6 TNBC patients) with different responses to chemotherapy was enrolled (validation cohort 1; Supplementary Table S4) and CD8$^+$ TILs were isolated from their primary tumors for bulk RNA-seq (Supplementary Fig. S1I). Consistent with the data from the discovery cohort, significantly more CD161$^+$CD8$^+$ TILs infiltrated chemoresistant tumors compared with the chemosensitive ones across all subtypes of breast cancer (Supplementary Fig. S1J and S1K).

CD161$^+$CD8$^+$ T cells are enriched in chemoresistant tumors

CD161 (encoded by *KLRB1*) is a C-type lectin that was initially identified to be expressed by NK cells (24). Nevertheless, its distribution in CD8$^+$ T cells has been known for decades, in not only unconventional T cells (25) like mucosal-associated invariant T (MAIT) cells and NKT cells but also some non-MAIT conventional CD161$^+$CD8$^+$ T cells (CD161$^+$ CTLs; refs. 26–29). Using the scRNA-seq data, we found that in C3_CD161 cells, semi-invariant TCRs characteristic of MAIT cells and NKT cells were not detected (Supplementary Fig. S2A). Instead, these cells exhibited great diversity in TCR Vαβ segments (Supplementary Fig. S2B). Some CD161$^+$ T cells have been reported to exhibit a Th17 phenotype (30, 31), but we found *IL17A* and *IL22* were rarely observed in C3_CD161 cells (Supplementary Fig. S2C). These findings corroborated that the CD161$^+$ cells enriched in chemoresistant tumors were not unconventional CD8$^+$ T cells.

After unconventional T-cell exclusion (Fig. 2A; Supplementary Fig. S2D), flow-cytometric analysis of tumor suspensions revealed that CD161 identified a CD8$^+$ T-cell subset that was notably increased in chemoresistant tumors compared with chemosensitive ones in all subtypes of breast cancer (Fig. 2B; Supplementary Fig. S2E and Supplementary Table S5). The specificity of the antibody was investigated by isotype control staining and staining of cells with CD161 introduction or deletion (Supplementary Fig. S2F). Furthermore, immunofluorescence staining of tumor sections, qRT-PCR, and western blot analyses of FACS-isolated cells from tumor suspensions verified the upregulation of CD161 within CD8$^+$ T cells of chemoresistant tumors (Fig. 2C–F; Supplementary Fig. S2G). Phenotypic analysis of the CD161$^+$ CTLs by flow cytometry revealed that they showed lower levels of markers associated with exhausted signatures like CTLA4, TIGIT, and TIM-3 than the CD161$^-$ counterparts. For costimulatory receptors, downregulation of 4-1BB but upregulation of DR3 were observed (Supplementary Fig. S2H). These findings suggested that the CD161$^+$CD8$^+$ T cells in breast cancer displayed a unique phenotype from classic exhausted T cells.

CD161 is preferentially expressed in tumor-specific CD8$^+$ T cells and associated with compromised T-cell cytotoxicity

Pentamer staining was used to identify tumor-specific CD8$^+$ T cells in HLA-A*02:01$^+$ breast cancer patients whose tumor cells overexpressed either the MUC1 or HER2 antigen (Supplementary Fig. S3A and S3B). By both MUC1 and HER2 pentamer staining, tumor-specific CD8$^+$ TILs were significantly less abundant in chemoresistant tumors

than chemosensitive ones (Supplementary Fig. S3C–S3E). Among chemoresistant patients, the proportion of CD161-expressing cells in MUC1 or HER2 pentamer$^+$ CTLs was significantly higher than that in their pentamer$^-$ counterparts (Fig. 3A and B; Supplementary Fig. S3F). Consistent with these data, immunofluorescence staining showed the expression of CD161 in pentamer$^+$ CTLs and its preferential distribution in tumor-specific T cells of chemoresistant patients (Fig. 3C and D).

CLEC2D, the ligand of CD161, is an inhibitory ligand for NK cells that restrains NK cell–mediated cytotoxicity after cross-linking CD161 (32, 33). In breast cancer patients, *CLEC2D* expression was observed in malignant cells by double staining with fluorescence *in situ* hybridization (FISH) for *CLEC2D* and immunofluorescence staining for EpCAM (Fig. 3E). Western blot analysis of EpCAM$^+$ cells from tumors confirmed the expression of CLEC2D in primary breast cancer cells (Fig. 3F; Supplementary Fig. S3G). Furthermore, chemoresistant tumors exhibited higher expression of CLEC2D than chemosensitive tumors (Fig. 3E and F; Supplementary Fig. S3G), suggesting potential roles for CLEC2D in immune escape and chemoresistance in breast cancer patients.

To investigate the contribution of the CD161–CLEC2D pathway to antitumor immunity, we expanded CD8$^+$ T cells from TILs with a standard small-scale REP (17, 34) and separated the CD161$^+$ and CD161$^-$ pentamer-stained T cells by FACS with the aforementioned gating strategy (Supplementary Fig. S3C and S3H). After dead cell removal, tumor cells were purified by MACS, and the CLEC2D$^+$ status was confirmed by flow cytometry before coculturing with autologous T cells (Supplementary Fig. S3I and S3J). Compared with the CD161$^-$ fraction, tumor-specific CD161$^+$ CTLs displayed compromised cytotoxicity to autologous neoplastic cells (Fig. 3G and H), with lower synthesis and secretion of proinflammatory cytokines, including IFNγ, perforin, granzyme B, and IL2 (Fig. 3I–K and Supplementary Fig. S3K). In summary, these data indicate that CD161 is predominantly expressed in tumor-specific CD8$^+$ TILs and associated with attenuated T cell–mediated anticancer responses in chemoresistant patients.

CD161 serves as an inhibitory receptor in tumor-specific CD8$^+$ T cells

To further investigate the functional significance of CD161, we generated two different coculture models (Fig. 4A). In the first system, CD161$^+$ CTLs were sorted from the peripheral blood of healthy donors (Supplementary Fig. S4A). Then, a CRISPR/Cas9 method was used to knock out CD161 (Supplementary Fig. S4B). A TCR recognizing the NY-ESO-1 antigenic peptide (NY-ESO-1:157–165 epitope) presented by HLA-A*02:01 was introduced into the sorted CD161$^+$ CTLs to generate NY-ESO-1–specific lymphocytes (ESO CTLs; Fig. 4B; Supplementary Fig. S4C). Flow-cytometric analysis showed that CD161 inactivation and NY-ESO-1 TCR introduction did not affect the phenotype of the T cells (Supplementary Fig. S4D). Then, we overexpressed NY-ESO-1 antigen and CLEC2D in MCF-7 breast tumor cells (Fig. 4C; Supplementary Fig. S4E), which are HLA-A2$^+$. In

Figure 6.
CD161 silencing in adoptive T-cell therapy potentiates antitumor responses and chemosensitivity in the PDXs. **A,** Schematic of the experimental design for two mouse models. **B,** Tumor growth curves of SYMHT02 PDXs in model A (top) and model B (bottom) with or without chemotherapy, T-cell transfer, or CD161 interference. **C,** Representative immunofluorescence images for TUNEL and CK in the xenografts in model B. Scale bar, 50 μm. See quantification in Supplementary Fig. S6D. **D,** Representative immunofluorescence images for CD8, IFNγ, and granzyme B in the xenografts in model B. Arrows denote CD8$^+$IFNγ$^+$ or CD8$^+$granzyme B$^+$ cells. Scale bar, 50 μm. See quantification in Supplementary Fig. S6E. **E,** ELISA for IL2 and IFNγ of CD8$^+$ T cells from PDXs in model B in response to autologous tumor cells. Results are mean ± s.e.m of $n = 3$ (model A) or 5 (model B) mice per group for each donor. *, $P < 0.05$; **, $P < 0.01$; ***, $P < 0.001$ by two-sided one-way ANOVA with the Tukey test.
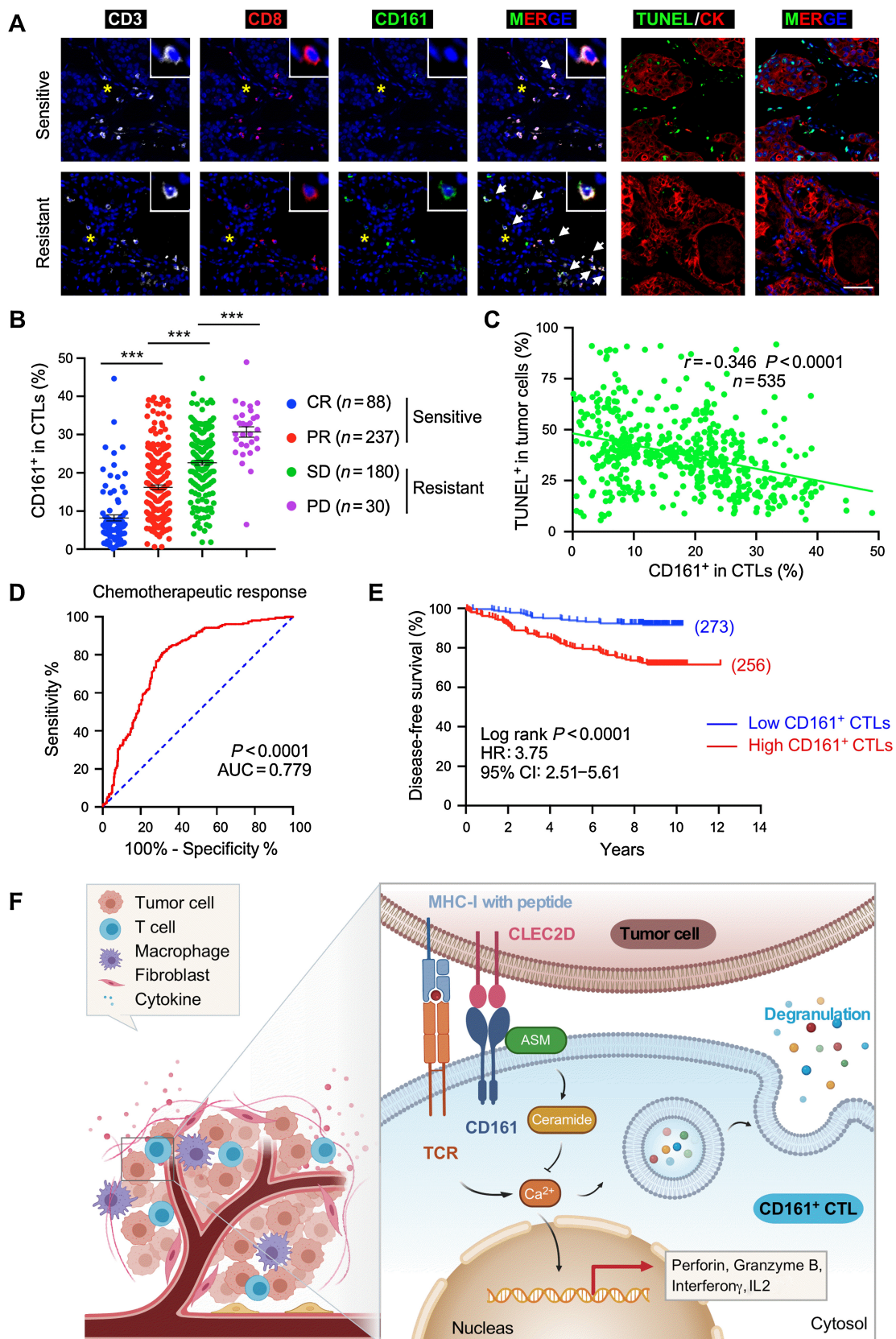
the second model, CD161 was knocked out in CD161$^+$ CTLs sorted from the initial outgrowth (pre-REP) of TILs, followed by a standard small-scale REP (**Fig. 4A**). The T cells were then cocultured with autologous tumor cells (**Fig. 4A**), which were confirmed to be CLEC2D$^+$ by flow cytometry (Supplementary Fig. S3J).

CD161 deletion reinforced the cytotoxic activity of both TIL-derived CD161$^+$ CTLs and ESO CTLs against tumor cells, whereas control treatment produced no such effect (**Fig. 4D** and **E**; Supplementary Fig. S4F and S4G). Furthermore, cellular degranulation and cytokine secretion of CD161^{KO} lymphocytes were upregulated relative to control-edited cells (**Fig. 4F** and **G**; Supplementary Fig. S4H). In addition, when HP-3G10, a CD161-specific monoclonal antibody, was applied to block CD161 in cocultures, T cells displayed strengthened cytotoxicity (**Fig. 4H** and **I**; Supplementary Fig. S4I) and cytokine release (Supplementary Fig. S4J and S4K). These observations shed light on the inhibitory effect of CD161 on T-cell functions and provide a rationale for the therapeutic potential of CD161-targeting strategies.

CD161 engagement blocks calcium influx in CTLs through ASM activation and ceramide generation

In NK cells, the cytoplasmic tail of CD161 interacts with and activates ASM after ligation (35). However, it has been reported that CD161 mediates distinct or even opposing effects on T cells and NK cells (32, 36). We, therefore, investigated whether ASM participates in the cross-linking of CD161 in CD8$^+$ T cells. After CD161 activation through microbeads loaded with an agonistic anti-CD161 antibody, confocal analysis of immunofluorescence staining showed that ASM colocalized with CD161 in TIL-derived CD161$^+$ CTLs (**Fig. 5A**). ASM is a fundamental enzyme in ceramide generation through the catabolic pathway (37). We found that the intracellular ceramide level in CD161$^+$ CTLs was remarkably upregulated in response to CD161 stimulation (**Fig. 5B**). These data supported the perspective that CD161 engagement in CTLs facilitated the activation of ASM and subsequent enhancement of ceramide production.

Ceramide has been implicated in the regulation of a variety of intracellular signaling pathways, including calcium mobilization (37). Calcium influx is crucial for lymphocytic functions, including not only T-cell activation, differentiation, and cytokine synthesis but also immune synapse formation and vesicle exocytosis (38, 39). Therefore, we examined the intracellular Ca^{2+} concentration following CD161 cross-linking. TCR stimulation resulted in prominent Ca^{2+} entry. But CD161 engagement curbed Ca^{2+} influx, and this was abrogated in CD161^{KO} CTLs (**Fig. 5C** and **D**; Supplementary Fig. S5A).

Next, we silenced ASM expression in CD161$^+$ CTLs using shRNA (Supplementary Fig. S5B). Knocking down ASM sharply decreased the production of ceramide (Supplementary Fig. S5C). In TIL-derived CD161$^+$ CTLs, silencing ASM abrogated the Ca^{2+} entry impediment induced by CD161 engagement (**Fig. 5E**; Supplementary Fig. S5D and S5E) and augmented the cytolytic effects of the T cells against autologous cancer cells (**Fig. 5F**). Similar results were obtained with the administration of imipramine, an ASM inhibitor (**Fig. 5G**;

Supplementary Fig. S5F and S5G). In contrast, reconstitution of ASM expression in ASM-knockdown cells restored ceramide levels, repressed Ca^{2+} influx and cytotoxic capacity of T cells (**Fig. 5H**; Supplementary Fig. S5H–S5J). These observations suggest that CD161 cross-linking in CTLs results in the subversion of calcium influx and impairments in cytotoxic functions through ASM activation and ceramide generation.

CD161 silencing in adoptive T-cell therapy potentiates antitumor responses and chemosensitivity in PDXs

To evaluate the therapeutic potential of CD161 targeting *in vivo*, we designed two mouse models (**Fig. 6A**), both of which were based on the inoculation of PDXs from breast cancer patients into immunocompromised NOD-SCID mice. PDX engraftment was successfully established with 3 of 19 fresh primary breast cancer resection samples (15.8%) from chemoresistant patients (Supplementary Table S6; Luminal B and TNBC subtypes). Paired blood samples and TILs were collected from the three patients. As shown by IHC staining, the major characteristics of the PDXs remained consistent with those of the original primary malignancies (Supplementary Fig. S6A). In model A, CD8$^+$ T cells isolated from patient blood were transduced with a CD161-overexpressing lentivirus and cocultured with blood-derived DCs pulsed with autologous tumor lysates (**Fig. 6A**). PDX-bearing mice received chemotherapy after palpable tumor formation. Then, we infused corresponding T cells and DCs into the mice through tail-vein injection. A blocking anti-CD161 or control IgG was administered intravenously 1 day before transfer and then every 3 days (Supplementary Fig. S6B). To generate a more humanized environment and better target CD161, in model B, CD161 was inactivated in TIL-derived CD161$^+$ CTLs by CRISPR/Cas9. After PDX establishment and chemotherapy, control or CD161^{KO} CTLs and autologous DCs were transfused into the PDX-bearing NOD-SCID mice with simultaneous and repetitive subcutaneous IL2 administration each day (**Fig. 6A**; Supplementary Fig. S6B).

Combining chemotherapy and CD161 silencing in T cells, through either genetic or pharmaceutical method, effectively retarded PDX growth (**Fig. 6B**; Supplementary Fig. S6C and S7A). As shown by immunofluorescence staining, targeting CD161 markedly upregulated cytokine production of CD8$^+$ TILs and increased the apoptosis of tumor cells (**Fig. 6C** and **D**; Supplementary Figs. S6D, S6E, and S7B-S7E), implying that CD161 silencing promoted antitumor immune responses. Without CD161 interventions, the application of chemotherapy failed to exert immunostimulatory effects on TILs. In contrast, silencing CD161 in mice receiving chemotherapy and CTL infusion resulted in robust cytotoxic immune responses and remarkable tumor cell death (**Fig. 6C** and **D**; Supplementary Figs. S6D, S6E, and S7B–S7E). These findings indicated that CD161 expression in CTLs prevented chemotherapy from inducing antitumor immunity activation, while targeting CD161 in tumor-specific CD8$^+$ T cells could work synergistically with chemotherapy to reinstate the immune benefits of chemotherapy and support anticancer immunosurveillance. Further

Figure 7.
CD161 expression in CTLs indicates poor therapeutic responses and patient outcomes. Paraffin tumor sections of 535 patients in validation cohort 2 were analyzed for CD161$^+$ CTL infiltration and its relation to tumor cell apoptosis and clinical outcomes. **A,** Representative immunofluorescent staining of CD3, CD8, CD161, CK, and TUNEL in breast cancer specimens. Arrows indicate CD161$^+$ CTLs. Scale bar, 50 μm. **B,** The proportions of CD161$^+$ CTLs in patients with different responses to chemotherapy (mean ± s.e.m.; CR, $n = 88$; PR, $n = 237$; SD, $n = 180$; PD, $n = 30$). **C,** Correlation between CD161 expression in CTLs and tumor cell apoptosis. **D,** Receiver operator characteristic (ROC) curves to predict neoadjuvant chemotherapeutic responses from intratumoral CD161$^+$ CTL enrichment. AUC, area under the curve. **E,** Kaplan–Meier survival curves for disease-free survival of breast cancer patients with low or high CD161$^+$ proportions of CD8$^+$ T cells. HR, hazard ratio. **F,** Schematic diagram of our main findings. $n = 535$ (**A–D**) or 529 (**E**) patients. P values were calculated by two-sided one-way ANOVA with Tukey test (**B**), two-tailed Pearson correlation coefficient test (**C**) or two-sided log-rank test (**E**).

analysis of cell disassociation from PDXs confirmed the successful targeting of CD161 in T cells (Supplementary Fig. S6F) and equivalent CLEC2D expression in xenograft tumor cells as primary cancer (Supplementary Fig. S6G). Mice receiving CD161-specific blocking antibody or control IgG exhibited a similar amount, proliferation, and apoptosis of CD161^{+} CTLs (Supplementary Fig. S7F–S7H), suggesting the antibody did not affect the survival of CD161^{+} cells *in vivo*. Moreover, functional analyses showed the enhanced production of cytokines like IFNγ and IL2 in T cells from mice receiving chemotherapy and CD161[KO] CTLs (**Fig. 6E**; Supplementary Fig. S6H). These data provide evidence that targeting CD161 serves as an effective anticancer approach for sensitizing recipients to chemotherapeutic treatments and limiting tumor development.

CD161 expression in CTLs indicates poor therapeutic responses and patient outcomes

To evaluate the clinical significance of CD161^{+} CTLs in mammary malignancies, we performed coimmunofluorescence staining for CD3, CD8, and CD161 in 535 breast cancer patients (validation cohort 2; **Fig. 7A**). CD161 expression in CD8^{+} TILs of patients resistant to neoadjuvant chemotherapy, that is, those with PD or SD after treatment, was conspicuously higher than that in patients who achieved CR or PR (**Fig. 7B**). Moreover, tumor cell apoptosis after chemotherapy exhibited a negative correlation with the level of CD161 in CTLs (**Fig. 7A** and **C**). A higher proportion of CD161^{+} CTLs in breast cancers was an independent variable associated with chemotherapeutic resistance (area under the receiver operating characteristic curve, 0.779; **Fig. 7D**). To further assess the association of CD161^{+} T-cell abundance with patient outcome, X-tile statistical software was applied to determine the optimal cutoff point. Enrichment of CD161^{+} CTLs within tumors was correlated with shorter patient disease-free survival (**Fig. 7E**), independent of breast cancer subtype (Supplementary Fig. S8A). And among the patients with low, moderate, and high total CD8^{+} T-cell infiltration, the upregulation of CD161 in CTLs was indicative of an adverse prognosis (Supplementary Fig. S8B). These observations suggest that high expression of CD161 in CD8^{+} TILs is associated with poor chemotherapeutic efficacy and patient prognoses in breast cancer.

In addition, we analyzed publicly available scRNA-seq data for 26 treatment-naïve breast cancers from GSE176078 (*14*). Consistent with our observations, the CD8^{+} T cells with higher CD161 expression exhibited a weaker cytotoxic signature (Supplementary Fig. S8C). Patients with a high proportion of CD161^{+}CD8^{+} cells showed compromised lymphocyte activation than those with low CD161^{+} CTL enrichment (Supplementary Fig. S8D–S8F). These observations verified and extended our conclusion that CD161 was associated with low immune efficacy (**Fig. 7F**).

Discussion

Given the role of immunologic clearance in the response to chemotherapy (*5, 6*), immune evasion exerts crucial influences on chemotherapeutic efficacy (*8*). Through single-cell dissection of the immune cell heterogeneity in primary breast cancers sensitive or resistant to neoadjuvant chemotherapy, we found that a subset of CD161-overexpressing CD8^{+} CTLs was dramatically enriched in chemoresistant tumors. Notably, CD161 was preferentially distributed in tumor-specific T cells and acted to inhibit cytotoxic effects through calcium influx blockade. Targeting CD161 potentiated the antitumor efficacy of tumor-specific lymphocytes and improved

chemosensitivity *in vivo*. This suggests an attractive prospect of combining CD161-based immune-activating interventions with chemotherapy or adoptive T-cell therapies to prevent immune evasion and reverse chemoresistance.

CD161 is expressed in several immune cells, including NK cells, CD4^{+} T cells, CD8^{+} T cells, and unconventional T cells such as MAIT cells, γδ T cells, and NKT cells (*27, 40–42*). CD161 expression in different types or clusters of cells can be related to different functional and prognostic significance (*29, 43, 44*). Prior studies found CD161 as a favorable prognostic factor in several cancers including breast cancer by pan-cancer resource computational analysis (*45*) and individual cancer studies (*46, 47*). However, some recent scRNA-seq analyses identified that CD161 was associated with adverse outcomes in diverse tumors (*48, 49*). CD161 was found characteristically expressed in the innate-like, low cytotoxic, and low clonal-expansive CD8^{+} TILs in early-relapsed liver cancer. These CD161^{+}CD8^{+} TILs failed to lyse recurrent tumor cells and inhibited the recruitment of effector CD8^{+} T cells, making an immune-evasive ecosystem (*49*). In addition, CD161 expression in chimeric antigen receptor (CAR) T cells was accompanied by a CD8^{+} T-to-NK-like transition and dysfunction (*50*). Blocking CD161 or its key regulators can enhance the tumoricidal capacity of CTLs against diffuse glioma (*48*) and pancreatic cancer (*50*), suggesting CD161 as an inhibitory receptor for antitumor CD8^{+} T-cell responses and a potential target to improve therapeutic effects (*48*). These studies suggest that neoplastic progression and therapeutic responses are closely linked to the heterogeneity of infiltrating immune cells, including cellular constitution, subpopulation distribution and molecular expression, which deserves further dissection. Herein, our single-cell landscape revealed that GZMK^{+}CD8^{+} CTLs were the most reduced subset in chemoresistant tumors compared with chemosensitive ones. In contrast, CD161^{+}CD8^{+} CTLs were markedly increased in chemoresistant tumors, suggesting the CD161^{+}CD8^{+} subset of CTLs as a protumor factor, unlike classic antitumor CTLs. Upon CLEC2D engagement, CD161 activated ASM and promoted ceramide production, ultimately inhibiting calcium influx and impairing cytotoxic functions. The abundance of CD161 in CD8^{+} T cells was associated with a poor prognosis in breast cancer. Importantly, interfering with CD161 was able to remodel the tumor immune microenvironment by changing the balance from protumor to antitumor effects for tumor-specific CTLs and thus serves as a tantalizing approach to improve chemotherapy.

Our findings identified a chemoresistance-associated CD161^{+} CD8^{+} T-cell subset and shed light on its immunosuppressive mechanism and therapeutic potential. Targeting CD161 can combat tumor immune evasion and resistance to chemotherapies or other immunogenic adjuvant treatments. In addition to its functions in tumors, CD161 participates in the attenuated cytotoxicity of T cells in infectious disease patients. CD161 is found in CD8^{+} T cells specific to hepatitis C virus, hepatitis B virus, human immunodeficiency virus, and Epstein–Barr virus (EBV), exhibiting impaired proliferation and cytolytic molecule production (*51–54*). These observations reveal that CD161-targeted strategies have the potential not only to improve the efficacy of immune-dependent antitumor treatments but also to boost host immune defense against exogenous pathogens. The enhancement of the antiviral T cell–mediated immune response is instrumental and imperative, especially today with the new coronavirus pandemic.

In summary, we reveal that a subset of CD161-overexpressing CD8^{+} T cells is enriched in chemoresistant tumors and associated with poor prognosis. Mechanistically, CD161 activates ASM and

ceramide generation in tumor-specific CTLs, mediating calcium influx blockade and T-cell dysfunction. These data highlight CD161 as an attractive therapeutic target to potentiate antitumor efficacy and reverse treatment resistance.

Authors' Disclosures

No disclosures were reported.

Authors' Contributions

L. Lao: Resources, data curation, software, formal analysis, writing–original draft, writing–review and editing. **W. Zeng:** Resources, data curation, formal analysis, investigation, writing–original draft, project administration, writing–review and editing. **P. Huang:** Data curation, software, formal analysis. **H. Chen:** Data curation, software, formal analysis. **Z. Jia:** Data curation, project administration. **P. Wang:** Resources, formal analysis. **D. Huang:** Validation, methodology. **J. Chen:** Data curation, formal analysis. **Y. Nie:** Investigation, methodology. **L. Yang:** Resources, data curation, validation, investigation. **W. Wu:** Methodology, writing–original draft, project administration, writing–review and editing. **J. Liu:** Conceptualization,

References

1. Vasan N, Baselga J, Hyman DM. A view on drug resistance in cancer. Nature 2019;575:299–309.
2. De Mattos-Arruda L, Shen R, Reis-Filho JS, Cortes J. Translating neoadjuvant therapy into survival benefits: one size does not fit all. Nat Rev Clin Oncol 2016; 13:566–79.
3. DeMichele A, Yee D, Esserman L. Mechanisms of resistance to neoadjuvant chemotherapy in breast cancer. N Engl J Med 2017;377:2287–9.
4. Ward RA, Fawell S, Floc'h N, Flemington V, McKerrecher D, Smith PD. Challenges and opportunities in cancer drug resistance. Chem Rev 2021;121: 3297–351.
5. Denkert C, Loibl S, Noske A, Roller M, Müller BM, Komor M, et al. Tumor-associated lymphocytes as an independent predictor of response to neoadjuvant chemotherapy in breast cancer. J Clin Oncol 2010;28:105–13.
6. Denkert C, von Minckwitz G, Darb-Esfahani S, Lederer B, Heppner BI, Weber KE, et al. Tumour-infiltrating lymphocytes and prognosis in different subtypes of breast cancer: a pooled analysis of 3771 patients treated with neoadjuvant therapy. Lancet Oncol 2018;19:40–50.
7. Galluzzi L, Buqué A, Kepp O, Zitvogel L, Kroemer G. Immunogenic cell death in cancer and infectious disease. Nat Rev Immunol 2017;17:97–111.
8. Topalian SL, Taube JM, Pardoll DM. Neoadjuvant checkpoint blockade for cancer immunotherapy. Science 2020;367:eaax0182.
9. Tauriello DVF, Sancho E, Batlle E. Overcoming TGFβ-mediated immune evasion in cancer. Nat Rev Cancer 2022;22:25–44.
10. Schmid P, Cortes J, Pusztai L, McArthur H, Kümmel S, Bergh J, et al. Pembrolizumab for early triple-negative breast cancer. N Engl J Med 2020; 382:810–21.
11. Mariya T, Hirohashi Y, Torigoe T, Asano T, Kuroda T, Yasuda K, et al. Prognostic impact of human leukocyte antigen class I expression and association of platinum resistance with immunologic profiles in epithelial ovarian cancer. Cancer Immunol Res 2014;2:1220–9.
12. Nanda R, Liu MC, Yau C, Shatsky R, Pusztai L, Wallace A, et al. Effect of pembrolizumab plus neoadjuvant chemotherapy on pathologic complete response in women with early-stage breast cancer: an analysis of the ongoing phase 2 adaptively randomized I-SPY2 trial. JAMA Oncol 2020;6:676–84.
13. Satija R, Farrell JA, Gennert D, Schier AF, Regev A. Spatial reconstruction of single-cell gene expression data. Nat Biotechnol 2015;33:495–502.
14. Wu SZ, Al-Eryani G, Roden DL, Junankar S, Harvey K, Andersson A, et al. A single-cell and spatially resolved atlas of human breast cancers. Nat Genet 2021; 53:1334–47.
15. Liberzon A, Birger C, Thorvaldsdóttir H, Ghandi M, Mesirov JP, Tamayo P. The molecular signatures database (MSigDB) hallmark gene set collection. Cell Syst 2015;1:417–25.
16. Jiang Y-Z, Ma D, Suo C, Shi J, Xue M, Hu X, et al. Genomic and transcriptomic landscape of triple-negative breast cancers: subtypes and treatment strategies. Cancer Cell 2019;35:428–40.
17. Rohaan MW, van den Berg JH, Kvistborg P, Haanen J. Adoptive transfer of tumor-infiltrating lymphocytes in melanoma: a viable treatment option. J Immunother Cancer 2018;6:102.
18. Tran KQ, Zhou J, Durflinger KH, Langhan MM, Shelton TE, Wunderlich JR, et al. Minimally cultured tumor-infiltrating lymphocytes display optimal characteristics for adoptive cell therapy. J Immunother 2008;31: 742–51.
19. Liu J, Lao L, Chen J, Li J, Zeng W, Zhu X, et al. The IRENA lncRNA converts chemotherapy-polarized tumor-suppressing macrophages to tumor-promoting phenotypes in breast cancer. Nat Cancer 2021;2:457–73.
20. Yang L, Liu Q, Zhang X, Liu X, Zhou B, Chen J, et al. DNA of neutrophil extracellular traps promotes cancer metastasis via CCDC25. Nature 2020;583: 133–8.
21. Huang D, Chen J, Yang L, Ouyang Q, Li J, Lao L, et al. NKILA lncRNA promotes tumor immune evasion by sensitizing T cells to activation-induced cell death. Nat Immunol 2018;19:1112–25.
22. Su S, Chen J, Yao H, Liu J, Yu S, Lao L, et al. CD10(+)GPR77(+) cancer-associated fibroblasts promote cancer formation and chemoresistance by sustaining cancer stemness. Cell 2018;172:841–56.
23. Huang D, Chen X, Zeng X, Lao L, Li J, Xing Y, et al. Targeting regulator of G protein signaling 1 in tumor-specific T cells enhances their trafficking to breast cancer. Nat Immunol 2021;22:865–79.
24. Yokoyama WM, Seaman WE. The Ly-49 and NKR-P1 gene families encoding lectin-like receptors on natural killer cells: the NK gene complex. Annu Rev Immunol 1993;11:613–35.
25. Pellicci DG, Koay HF, Berzins SP. Thymic development of unconventional T cells: how NKT cells, MAIT cells and γδ T cells emerge. Nat Rev Immunol 2020; 20:756–70.
26. Lanier LL, Chang C, Phillips JH. Human NKR-P1A. A disulfide-linked homodimer of the C-type lectin superfamily expressed by a subset of NK and T lymphocytes. J Immunol 1994;153:2417–28.
27. Fergusson JR, Smith KE, Fleming VM, Rajoriya N, Newell EW, Simmons R, et al. CD161 defines a transcriptional and functional phenotype across distinct human T cell lineages. Cell Rep 2014;9:1075–88.
28. Fergusson JR, Fleming VM, Klenerman P. CD161-expressing human T cells. Front Immunol 2011;2:36.
29. Konduri V, Oyewole-Said D, Vazquez-Perez J, Weldon SA, Halpert MM, Levitt JM, et al. CD8+CD161+ T-cells: cytotoxic memory cells with high therapeutic potential. Front Immunol 2020;11:613204.
30. Maggi L, Santarlasci V, Capone M, Peired A, Frosali F, Crome SQ, et al. CD161 is a marker of all human IL-17-producing T-cell subsets and is induced by RORC. Eur J Immunol 2010;40:2174–81.
31. Cosmi L, De Palma R, Santarlasci V, Maggi L, Capone M, Frosali F, et al. Human interleukin 17-producing cells originate from a CD161+CD4+ T cell precursor. J Exp Med 2008;205:1903–16.

32. Aldemir H, Prod'homme V, Dumaurier M-J, Retiere C, Poupon G, Cazareth J, et al. Cutting edge: lectin-like transcript 1 is a ligand for the CD161 receptor. J Immunol 2005;175:7791–5.

33. Rosen DB, Bettadapura J, Alsharifi M, Mathew PA, Warren HS, Lanier LL. Cutting edge: lectin-like transcript-1 is a ligand for the inhibitory human NKR-P1A receptor. J Immunol 2005;175:7796–9.

34. Ye Q, Song D-G, Poussin M, Yamamoto T, Best A, Li C, et al. CD137 accurately identifies and enriches for naturally occurring tumor-reactive T cells in tumor. Clin Cancer Res 2014;20:44–55.

35. Pozo D, Valés-Gómez M, Mavaddat N, Williamson SC, Chisholm SE, Reyburn H. CD161 (human NKR-P1A) signaling in NK cells involves the activation of acid sphingomyelinase. J Immunol 2006;176:2397–406.

36. Exley M, Porcelli S, Furman M, Garcia J, Balk S. CD161 (NKR-P1A) costimulation of CD1d-dependent activation of human T cells expressing invariant V alpha 24 J alpha Q T cell receptor alpha chains. J Exp Med 1998;188:867–76.

37. Adam D, Heinrich M, Kabelitz D, Schütze S. Ceramide: does it matter for T cells? Trends Immunol 2002;23:1–4.

38. Feske S. Calcium signalling in lymphocyte activation and disease. Nat Rev Immunol 2007;7:690–702.

39. Lyubchenko TA, Wurth GA, Zweifach A. Role of calcium influx in cytotoxic T lymphocyte lytic granule exocytosis during target cell killing. Immunity 2001;15: 847–59.

40. Legoux F, Salou M, Lantz OJI. MAIT cell development and functions: the microbial connection. Immunity 2020;53:710–23.

41. Crosby CM, Kronenberg M. Tissue-specific functions of invariant natural killer T cells. Nat Rev Immunol 2018;18:559–74.

42. Godfrey DI, Stankovic S, Baxter AG. Raising the NKT cell family. Nat Immunol 2010;11:197–206.

43. Duurland CL, Santegoets SJ, Abdulrahman Z, Loof NM, Sturm G, Wesselink TH, et al. CD161 expression and regulation defines rapidly responding effector CD4+ T cells associated with improved survival in HPV16-associated tumors. J Immunother Cancer 2022;10:e003995.

44. Braud VM, Meghraoui-Kheddar A, Elaldi R, Petti L, Germain C, Anjuère F. LLT1-CD161 interaction in cancer: promises and challenges. Front Immunol 2022;13:847576.

45. Gentles AJ, Newman AM, Liu CL, Bratman SV, Feng W, Kim D, et al. The prognostic landscape of genes and infiltrating immune cells across human cancers. Nat Med 2015;21:938–45.

46. Braud VM, Biton J, Becht E, Knockaert S, Mansuet-Lupo A, Cosson E, et al. Expression of LLT1 and its receptor CD161 in lung cancer is associated with better clinical outcome. Oncoimmunology 2018;7:e1423184.

47. Santegoets SJ, van Ham VJ, Ehsan I, Charoentong P, Duurland CL, van Unen V, et al. The anatomical location shapes the immune infiltrate in tumors of same etiology and affects survival. Clin Cancer Res 2019;25: 240–52.

48. Mathewson ND, Ashenberg O, Tirosh I, Gritsch S, Perez EM, Marx S, et al. Inhibitory CD161 receptor identified in glioma-infiltrating T cells by single-cell analysis. Cell 2021;184:1281–98.

49. Sun Y, Wu L, Zhong Y, Zhou K, Hou Y, Wang Z, et al. Single-cell landscape of the ecosystem in early-relapse hepatocellular carcinoma. Cell 2021;184:404–21.

50. Good CR, Aznar MA, Kuramitsu S, Samareh P, Agarwal S, Donahue G, et al. An NK-like CAR T cell transition in CAR T cell dysfunction. Cell 2021;184: 6081–100.

51. Northfield JW, Kasprowicz V, Lucas M, Kersting N, Bengsh B, Kim A, et al. CD161 expression on hepatitis C virus-specific CD8+ T cells suggests a distinct pathway of T cell differentiation. Hepatology 2008;47:396–406.

52. Billerbeck E, Kang Y-H, Walker L, Lockstone H, Grafmueller S, Fleming V, et al. Analysis of CD161 expression on human CD8+ T cells defines a distinct functional subset with tissue-homing properties. Proc Nat Acad Sci USA 2010;107:3006–11.

53. Dominguez-Molina B, Ferrando-Martinez S, Tarancon-Diez L, Hernandez-Quero J, Genebat M, Vidal F, et al. Immune correlates of natural HIV elite control and simultaneous HCV clearance-supercontrollers. Front Immunol 2018;9:2897.

54. Poon K, Montamat-Sicotte D, Cumberbatch N, McMichael AJ, Callan MF. Expression of leukocyte immunoglobulin-like receptors and natural killer receptors on virus-specific CD8+ T cells during the evolution of Epstein–Barr virus-specific immune responses in vivo. Viral Immunol 2005;18:513–22.